Biogeosciences Discuss., 11, 281–336, 2014
www.biogeosciences-discuss.net/11/281/2014/
doi:10.5194/bgd-11-281-2014

Biogeosciences Discussions
Open Access

The Black Sea biogeochemistry: focus on temporal and spatial variability of oxygen

E. V. Stanev[1], Y. He[1,2], J. Staneva[1], and E. Yakushev[3]

[1]Helmholtz-Zentrum Geesthacht, Max-Planck-Straße 1, 21502 Geesthacht, Germany
[2]Institut für Geowissenschaften, Universität Kiel, Ludewig-Meyn-Str. 10, 24118 Kiel, Germany
[3]Norwegian Institute for Water Research, Gaustadalleen 21, 0349 Oslo, Norway

Received: 6 December 2013 – Accepted: 12 December 2013 – Published: 7 January 2014

Correspondence to: E. V. Stanev (emil.stanev@hzg.de)

Published by Copernicus Publications on behalf of the European Geosciences Union.

Abstract

The temporal and spatial variability of the upper ocean hydrochemistry in the Black Sea down to its suboxic zone was analyzed using data originating from historical observations, profiling floats with oxygen sensors and numerical simulations carried out with a coupled three-dimensional circulation-biogeochemical model including 24 biochemical state variables. The validation of the numerical model against observations demonstrated that it replicated in a realistic way the statistics seen in the observations. The suboxic zone shoaled in the central area and deepened in the coastal area, which was very well pronounced in winter. Its depth varied with time in concert with the variability of the physical system. Two different regimes of ventilation of the pycnocline were clearly identified: gyre-dominated regime in winter and eddy dominated regime in summer. These contrasting regimes were characterized by very different pathways of oxygen intrusions along the isopycnals. The contribution of the three-dimensional modeling to the understanding of the Black Sea hydro-chemistry, and in particular the coast-to-open-sea diapycnal mixing was also demonstrated.

1 Introduction

The Black Sea (Fig. 1) is the world's largest marine anoxic basin (Skopintsev, 1975; Murray et al., 1989; Sorokin, 1982; Jørgensen et al., 1991; Murray et al., 1995). Anoxic conditions formed about 8000 yr ago because of the reconnection of Mediterranean and Black Sea and the intrusion of saltier Mediterranean water which followed the reconnection (Deuser, 1974). The micro-structure profiling measurement (Gregg and Yakushev, 2005) revealed extremely low vertical turbulent exchange (coefficients of about $1–4 \times 10^{-6}\ m^2\ s^{-1}$), which explained the strong vertical stratification (Fig. 2) represented by an oxygenated surface layer and a sulfide containing deep layer (Oguz et al., 2005). The oxic and sulfidic waters are separated by a layer between the isopycnal depths σ_t = 15.40 and 16.20 known as the suboxic zone (Murray et al., 2005). This

BGD
11, 281–336, 2014

zone was defined by Murray et al. (1989, 1995) as the water layer where concentrations of both dissolved oxygen and hydrogen sulfide were below detection limit. The suboxic zone is an important biogeochemical interface between the surface and deep waters. The processes controlling its origin and variability have been extensively discussed by Saydam et al. (1993), Basturk et al. (1994), Yakushev et al. (1997, 2007). Murray et al. (1989) suggested first that the suboxic zone might be a new feature caused by the reduced fresh water input from rivers and the resulting change in the ventilation, but Buesseler et al. (1994) proved that the suboxic zone was most likely a permanent feature in the Black Sea. Latter, Konovalov and Murray (2001) demonstrated that the depth of the upper boundary of suboxic zone was governed by the balance between the ventilation of thermocline with oxygen-rich surface water and oxygen-consumption by the oxidation of organic matter.

The sensitivity of the suboxic zone upon the physical drivers was revisited by the numerical experiments of Yakushev et al. (1997, 2009) who demonstrated the role of the cycling of nitrogen-manganese-iron-sulfur elements. ANaerobic AMMonium OXidation (Anammox process), in which nitrite ions were utilized by bacteria to oxidise ammonium and produce nitrogen gas seems to be the single but most important suboxic respiratory pathway in the water column (Kuypers et al., 2003). Within the oxygen deficient part of the water column, de-nitrification results in a sharp decrease of the nitrate concentration (Fig. 2c and f) from the peak to trace values and zero concentrations around 110 m. Below the suboxic zone, hydrogen sulfide and ammonium were found in high concentration filling the anoxic zone down to the bottom (Fig. 2b and e).

A series of complicated redox processes take place in this transition zone, the manganese cycling is one of the most important ones (Murray et al., 1995; Rozanov, 1995; Yakushev et al., 2006). This cycling process in which reduced Mn can be oxidized only by oxygen, while oxidized forms of Mn can be reduced by sulfide and iron was first incorporated in a biogeochemical model by Yakushev (1998) and latter implemented in the model that took into account an enhanced sinking rate of the Mn particles (Debolskaya and Yakushev, 2002).

BGD
11, 281–336, 2014

The temporal and spatial variability of the suboxic zone reflects fundamental changes associated with the sulfide production in the water column and sulfide oxidation at the base of the suboxic zone, as well as feedback mechanisms crucial for the entire Black Sea ecosystem (Neretin et al., 2001). However, the earlier research did not enough address the temporal and spatial variability because of the insufficient amount of observations. The present paper aims at demonstrating that continuous biogeochemistry observations over large areas and coupled 3-dimensional circulation-ecosystem numerical modeling can advance our understanding in this field. We admit that the use of the term "biogeochemistry" in our study does not equally focus on all compartments of the Black Sea system. In the middle of our research focus is oxygen and hydrogen sulfide, as well as some other directly connected to them variables. The reason for that is that we: (1) focus on the general and most pronounced patterns, which are characteristic for the entire basin, and (2) we want to use in a coherent way high-resolution in time and space observations in parallel with numerical simulations. The recent observational activities using Argo floats equipped with oxygen sensors provide such data. Another argument not to address all possible aspects of temporal and spatial characteristics of Black Sea biogeochemistry is the research focus in this paper, which is on the physical impacts on the biogeochemistry, in particular of the diapycnic mixing. Deeper insight in the coastal processes and individual biogeochemistry parameters will be given in future publications.

To the best of our knowledge the 3-D numerical modeling of the Black Sea hydrochemistry was initiated for more than twenty years (Stanev, 1989), however, the model used in this study was extremely simple (only oxygen and hydrogen sulfide were simulated) and the resolution was very coarse. In the following two decades two important development happened: (1) the 1-D modeling gained larger maturity (Oguz et al., 1996, 2000, 2001; Oguz, 2002; Yakushev, 1992; Yakushev and Neretin, 1997; Yakushev et al., 2007; Lancelot et al., 2002; Gregoire et al., 2008; Gregoire and Soetaert, 2010), and (2) the quality of the 3-D modeling improved substantially by using more complex and realistic models and much better resolution (Gregoire et al., 1997, 1998; Staneva et al.,

BGD
11, 281–336, 2014

1998; Stanev et al., 2001; Oguz et al., 2002; Gregoire and Lacroix, 2003; Capet et al., 2013). Recently the 3-D ecosystem modeling was implemented in the Black Sea operational oceanography (Korotaev et al., 2011).

Although the Black Sea has been used as the major playground to test development of the modelling of dissolved oxygen and hypoxia dynamics (Pena et al., 2010), there are still a number of open questions. Two of them are: (1) what is the affordable with the available computational power model vertical and horizontal resolution which would guarantee reasonable simulations, (2) what is the consistence of the numerical simulations with continuous observations. The answers of (1) and (2) could open the discussion of the needed sampling capabilities of available observational platforms and design of appropriate models. The present study tries to make one step in this direction. However, there is one very basic question to answer first: (3) which are the important features in the dynamics of oxygenated and sulfide water, which can not be understood fully using available data and simple one-dimensional concepts. One such concept is the assumption that tracers in the Black Sea well follow the isopycnals (Stanev et al., 2004), that is the vertical stratification in density coordinates (one profile only) adequately represents the entire basin. An answer of (3) will be given in the present study based on the analysis of 3-D numerical simulations.

The specific research objectives of this paper are to (1) describe the coupling of the 1-D Redox Layer Model (ROLM, Yakushev et al., 2006) with a 3-D numerical circulation model (General Estuarine Ocean Model, GETM) and address some numerical issues, (2) describe the temporal and spatial variability of oxygen as seen in historical data, profiling floats observations and numerical simulations, (3) address the spatial and temporal distributions of oxygen and hydrogen sulfide in the suboxic zone, (4) identify future developments needed in this field. The paper is organized as follows. Section 2 presents a brief analysis of the Black Sea hydrochemistry. The used physical and biogeochemical models are described in Sect. 3 and Appendix A. Section 4 describes the model validation against observations followed by analyses of the major results in Sect. 5 and short conclusions.

BGD
11, 281–336, 2014

2 Historical observations: overall description of the Black Sea hydrochemistry

Historical data plotted against density in Fig. 3 revealed a spread of the observations in the upper layers down to σ_θ = 14. This isopycnic level was close to the upper boundary of Cold Intermediate Layer (CIL). Above this boundary the dynamics of the upper mixed layer and seasonal thermocline were dominating, explaining the large variability seen in the oxygen content. An overall linear relationship between oxygen and density was characteristic for the upper halocline (between σ_θ = 14.2 and 15.2). The rapid decrease of oxygen concentrations at below σ_θ = 15.3 represented the transition to anoxic conditions that is the lower boundary of the Black Sea aerobic zone. These historical profiles are consistent with observations by Stanev et al. (2013) who analyzed data from continuous profiling Argo floats during 2010–2012. This consistence excludes misinterpretations associated with errors in historical data. However, what also became clear from this study was that the oxygen stratification was stronger in the interior part of the Black Sea and weaker in the coastal zone, that is the above data, which correspond to the open-ocean conditions give just a first order presentation of oxygen stratification.

The linear relationship between oxygen and σ_θ resembles similar relationships found for other passive tracers (Stanev et al., 2004). What was not so clear in the past was that similar line approximates the relationship between hydrogen sulfide and σ_θ below σ_θ = 16.5 hat is in the deeper layers the sulfide distribution is characterized by a linear increase of concentrations down to σ_θ = 17.2.

The oxygen curve in historical observations was shifting periodically towards lower or higher density in the last 50 yr, while the gradient remained the same. Noteworthy is that the changes in the transition layer as seen in σ_θ coordinates did not show a clear shift up and down like this was the case in the oxygenated layer. This gives an indication that the long-term changes of the Black Sea hydrochemistry in the transition zone are not trivially linked to the ones in the oxygen and sulphide dominated layers. In summary,

BGD
11, 281–336, 2014

the recent changes in the Black Sea hydrochemistry were better seen down to the suboxic zone (see for further detail Stanev et al., 2013) but not in the deep layers.

The oxygen and sulphide profiles in σ_θ coordinates can be presented as a unique O_2–H_2S curve (Fig. 3), which resembles the variable $D = aO_2 - H_2S$ introduced by Stanev (1989), where a is a stoichiometric constant. The O_2–H_2S curve undergoes a jump between $\sigma_\theta = 15.4$ and 16.5, that is, in the transition zone between the layers where oxygen is the dominant oxidizer, and sulfide is the dominant reducer (redox zone). This redox layer combines oxygen-deficient, hypoxic, suboxic (suboxidized and subreduced) and anoxic conditions (Yakushev and Newton, 2013). Obviously, Fig. 3 gives a nice illustration of the fact that the suboxic zone has the typical characteristics of a boundary layer, which becomes very clear if data are analysed in density coordinates. This "jump" is intimately associated with the diapycnal mixing caused by chemical transformations of matter because in this redox layer there are different oxydizers such as nitrate, Mn(IV), Fe(III), reducers such as NH_4, Mn(II), Fe(II) and intermediate species acting as oxydizers or reducers (NO_2, Mn(III), S_2O_3, S_0). Without going here in deeper details of diapycnic mixing it is worth mentioning that in the linear section of the profiles in Fig. 3, O_2 and H_2S are mixed (transported) but not consumed. The curvature would indicate stronger consumption (sources) that is the diapycnal processes (or matter transformation) are localized in the suboxic layer (see McDougall, 1984).

The analysis of continuous observations by Stanev et al. (2013) and the discussion above proved that in the upper halocline the oxygen distribution followed the one of density. This means that in these layers the assumption of density-oxygen alignment holds. However, below the linear part of the profiles in Fig. 3 where the scatter in data was large and the mean oxygen concentrations small the assumption of density alignment was not valid basin-wide. Therefore, extending the interpretations of local observations in the suboxic zone basin-wide should be made carefully. As shown in. Figure 3 the density–sulfide relationship below the suboxic zone is also stable, which gives more confidence to the analyses of scarce historical observations in deeper layers.

BGD
11, 281–336, 2014

The Black Sea hydrochemistry stratification demonstrated above motivated researchers to use density (salinity) coordinates to describe the overall distribution of properties (Vinogradov and Nalbandov, 1990; Konovalov et al., 2005). This presentation reduced the data-scatter seen in depth coordinates, and rendered analyses quasi-independent from the specific location (Stanev et al., 2004). Analyses in density coordinate have also been extensively used to evaluate the variability of physical and biogeochemical contents in 1-D models (Oguz et al., 1996, 2000, 2001; Oguz, 2002; Yakushev and Neretin, 1997; Yakushev et al., 2007). It is instructive, before moving to the 3-D numerical modelling, to ask the following question: provided the robust relationship between oxygen and density in the area of the pycnocline exists, can mapping the "standard" profiles (e. g. the mean profile from Fig. 3) in the 3-D space and time ensure a realistic reconstruction of temporal and spatial patterns. A comparison between this simplified "reconstruction" approach and the 3-D simulations would then reveal the benefit of using 3-D models. The observations using Argo floats equipped with oxygen sensors (Stanev et al., 2013) gave a preliminary guidance to answering this question. According to these data the slope of oxygen curve in the coastal zone was much smaller than one in the open ocean. These results demonstrated that it was not only the linear part of the historical profiles shifting up and down, but also the differences in the oxygen stratification between coastal and open sea were substantial.

3 The numerical model

3.1 Model description

The hydrodynamic model GETM (General Estuarine Transport Model) solves the equations for the three velocity components u, v and w, temperature T, salinity S and sea surface height ζ, as well as the equations for turbulent kinetic energy and the eddy dissipation rate due to viscosity. The governing equations and numerics are presented by Burchard and Bolding (2002). The implementation of GETM to the Black Sea has been

BGD
11, 281–336, 2014

described by Peneva and Stips (2005). The circulation model is coupled with the ROLM (RedOx Layer Model). The redox processes implemented in this model were first modelled by Yakushev and Neretin (1997) with a focus on the nitrogen and sulphur cycles. In their model the sulphur cycle was driven by a continuous supply of oxygen caused by a downward diffusive oxygen flux. Debolskaya and Yakushev (2002) advanced the model by incorporating a simplified manganese cycling in which the particulate manganese was used for oxidizing the hydrogen sulfide, and the dissolved manganese was oxidized by oxygen. Yakushev et al. (2006) added in ROLM a parameterization of the processes of formation of organic matter during both photosynthesis and chemosynthesis (Fig. 4).

ROLM coupled with the General Ocean Turbulence model (GOTM, Burchard et al., 2005) proved to be an efficient tool to simulating the main features of biogeochemical structure of the redox interfaces (Yakushev et al., 2006, 2011). Figure 4 gives a flow chart of the biogeochemical processes addressed in this model. The names of variables are given in Table A1.

In its 1-D version ROLM uses vertical diffusion equations for non-conservative substances:

$$\frac{\partial C_i}{\partial t} = \frac{\partial}{\partial z}\left(A_V^C \frac{\partial C_i}{\partial z}\right) - \frac{\partial((W_C + W_{Mn})C_i)}{\partial Z} + R_{C_i}, \quad (1)$$

where C_i is the concentration of "ith" model variable, A_V^C is the vertical turbulent diffusion coefficient for biogeochemistry tracers, which is assumed to be equal to the vertical turbulent diffusion coefficient for temperature and salinity $A_V^{(T,S)}$, W_C is the sinking velocity of particulate matter, W_{Mn} – accelerated velocity of sinking of particles with Mn hydroxides. The term $R_{Ci} = \sum_j \mathrm{Rate}_{BjCi}$ which is presented as an algebraic sum of local fluxes (sources and sinks) caused by biogeochemical interaction (Rate_{BjCi}) describes the rate of biogeochemical production and consumption of Ci, by Bi. The parameterization of the biogeochemical processes was described by Yakushev et al. (2007).

BGD
11, 281–336, 2014

In the present paper the one-dimensional coupled Black Sea GOTM-ROLM (He et al., 2012) is implemented in GETM. Because the biogeochemical part used here is essentially the same as in the above study, only some details concerning the vertical resolution and model performance are presented in Appendix A. From these results it follows that a very fine vertical resolution of about 2 m was needed to realistically simulate the biogeochemical process in the upper 150 m. Keeping in the 3-D model a resolution of 2 m that is about 1000 vertical levels in the deep part of the sea (around 2000 m deep) is a big computational challenge. Due to this reason a simplified approach to the modelling of the Black Sea hydrochemistry is proposed in the following: (1) focus on the upper ocean down to 200 m, which enables to address with sufficient vertical resolution the dynamics of suboxic zone and, (2) use an optimal horizontal resolution, which is fine enough to simulate basic circulation features of the Black Sea. Said in other words, the compromise proposed here neglects the deep-sea processes (substitutes them with an appropriate boundary condition) in favour of the ones down to the pycnocline, where the suboxic zone dynamics presents the major research interest.

3.2 Model set up

The model is set up for the upper 200 m with 2 m vertical resolution as in the 1-D model (see Appendix A). The model was set up with a horizontal resolution of $1/10^{\circ}$ in longitude and $1/12^{\circ}$ in latitude, and used essentially the same grid as the one used by Stanev et al. (2003) who addressed the water mass formation simulated with the Modular Ocean Model (MOM). Grayek et al. (2010) and Stanev and Kandilarov (2012) used the same grid in their set up based on the Nucleus for European Modelling of the Ocean, which they applied to data assimilation and sediment dynamics, respectively.

The model topography was prepared based on the one used in the above studies. It has a minimum depth of 20 m (as in the original data set) and was modified in a way that the maximum depth was changed to 200 m. Below 120 m the topography was smoothed in order to allow a smooth transition between the steep continental slope and the basin interior.

BGD
11, 281–336, 2014

For the ordinary differential equations solver to calculate the biogeochemical process the First-order Extended Modified Patankar scheme was used, which is stoichiometrically conservative (see also He et al., 2012). The selected advection scheme for tracers is the first order upstream in the horizontal and ultimate quickest Total Variance Dissipation formulation (TVD) in the vertical.

Parameters used in ROLM are the same as in the 1-D model (see He et al., 2012). Several sensitivity experiments have been carried out using different values for the background diffusivity coefficients and sinking velocity, which replicated well the sensitivity experiments discussed by Yakushev et al. (2007, 2009).

3.3 Boundary conditions

At the sea surface atmospheric parameters (air temperature, air humidity, sea level pressure, 10 m wind and total cloud cover) were taken from the atmospheric analysis data. These data, along with the calculated in the model solar radiation and simulated from the model SST, are used to compute heat and momentum fluxes. The atmospheric analysis data were provided from the European Center for Medium-Range Weather Forecasts (ECMWF) with a horizontal resolution of approximately ($0.2^{\circ} \times 0.2^{\circ}$). The computation of fluxes used bulk formulas (see Grayek et al., 2011 for the used equations and parameters).

Like in the 1-D model the flux of oxygen at sea surface was computed as depending on the difference in partial pressure of oxygen between air and the surface and on a transfer coefficient, which was a function of wind speed and sea surface temperature (Appendix A). The formulation of fluxes of nutrients and phosphorus used the values given in Appendix A distributed among the major rivers as described by Stanev and Kandilarov (2012). For the remaining biogeochemical state variables air–sea interface was considered as impermeable. The bottom values were relaxed to climatological temperature and salinity. For the remaining tracers the bottom boundary condition used the data described in Appendix A (as a function of density). These data were mapped in time and 3-D space following the concept of isopycnal alignment, which is applicable

BGD
11, 281–336, 2014

below the suboxic layer (see Sect. 2), and the resulting values at the model bottom were used as bottom boundary conditions.

3.4 Model initialization and simulations

The Biogeochemical and physical models are on-line coupled with time step of 15 s. The integration was started from rest using as initial condition the vertical profiles simulated in the 1-D model, that is horizontally homogenous initial data have been imposed for temperature, salinity and all 24 biogeochemical state variables (see Appendix A and Table A1). Cyclic atmospheric forcing as described by He et al. (2012) was used until a quasi-steady state was reached. The integration was then continued for the studied period with the atmospheric forcing presented in Sect. 3.3. The model runs analyzed in this paper cover the period 2008–2012, the time after 2010 overlaps with the time when continuous observations from profiling floats have been collected. Most of analyses will be shown for 2010.

4 Overall presentation of the numerical simulations

4.1 Upper ocean patterns

The simulated February-mean SST in 2010 (Fig. 5a) was lower than 8 °C over the western and central Black Sea reaching 10 °C around the eastern coast. This enabled cold intermediate water to form over large areas (for the water mass formation in the Black Sea see Stanev et al., 2003). The lowest SST was simulated in the northwestern shelf; this low-temperature area was extending southward because of the transport along the western coasts.

The surface oxygen pattern (not shown here because it is very similar to that at 20 m which we analyze in the following) was almost opposite to the distribution of SST due to the negative correlation between the two. However, the gradients were much stronger

BGD
11, 281–336, 2014

than in the SST and more affected by the hydrodynamics (see the tongue-like coast-guided pattern in Fig. 5c along the eastern Black Sea coast). The difference between the surface and saturated oxygen concentration displays the pattern of air-sea oxygen flux (Fig. 5b). Obviously this field revealed signatures of coastal currents and some eddy-like structures, as the meander west of the Crimea Peninsula.

The highest oxygen values were simulated in the northwestern shelf area (Fig. 5c). Obviously the minimum in the air-temperature in this region was the major reason for this anomaly. Similarly, the eastern coast guided the propagation of the low-oxygen water. With the increasing depth the distribution of O_2 did not change down to 20 m, however at 40 m the patterns were rather different (Fig. 5d). At this depth, the oxygen values in the eastern Black Sea dropped to about 200 µM, which was associated with the vertical circulation bringing low-oxygen water into the surface layer. From the above analysis it seems obvious that the spatial variability, which was missing in the 1-D models (He et al., 2012) could substantially impact the oxygen dynamics.

4.2 The thermohaline fields

The numerical simulations compare well with the ones reported by Stanev et al. (2003), Grayek et al. (2010) and Stanev and Kandilarov (2012), which used the same horizontal grid, as well as with the ones originating of the GETM application for the Black Sea of Peneva and Stips (2005). This is the reason why the simulated hydrodynamics will not be extensively addressed here leaving more place to present details on the modelling of hydrochemistry. The simulated circulation was predominantly cyclonic and structured in persistent western and eastern gyre. The currents, the main current is known as the Rim Current, were stronger in winter than in summer supporting the earlier analyzes from numerical models (e.g. Staneva et al., 2001). Some dominant signatures in the circulation patterns are described in more detail further in the text when the impact of circulation on the biogeochemistry is presented. Among them is the strong meander west of the Crimea Peninsula, which could be considered as the model analogue of

BGD
11, 281–336, 2014

the Crimea Eddy. The second important subbasin scale eddy (the Batumi eddy) was better pronounced in summer.

The CIL in the Black Sea (Fig. 6) is a permanent layer at 50–100 m (see also Fig. 2a and Fig. 2d) acting as a near-surface thermal reservoir, similar to the North Atlantic Subtropical Mode Water, which is renewed due to vertical mixing during cold winters (Stanev et al., 2003; Gregg and Yakushev, 2005). Winter cooling penetrated down to about 100 m in the western Black Sea (Fig. 6). Cold water extended over almost the entire basin. Only in the eastern most regions the SST was higher than the temperature in the deeper layers. In summer the cold water was overlain by the warm surface water forming the CIL (Fig. 6b). The CIL was noticeable until the next winter, giving a clear signature of how persistent this water mass was. The variations in the depth of its lower boundary correlated with the oscillations of the depth of the pycnocline (compare the upper and bottom panels in Fig. 6). Its thickness in the central basin was smaller than in the coastal zone reflecting the impact of upwelling and downwelling, respectively. The temperature in the core of CIL was in most cases higher than 8 °C, which did not support the usually accepted definition of Blatov et al. (1984) describing the CIL as a permanent layer at 50–100 m with temperatures lower than 8 °C. However this gave a modeling support to the recent finding of Stanev et al. (2013) that for the considered period the cold intermediate water was substantially warmer than previously known.

At the base of the CIL the main pycnocline, which was mostly due to the strong vertical salinity gradients, acted as an obstacle for the propagation of temperature signal in the deeper layers. Therefore the lower boundary of the CIL followed the topography of pycnocline. The stronger dooming of the pycnocline in winter reflected the known winter intensification of the Black Sea circulation (see also Stanev et al., 2003).

With respect to the surface thermal properties the seasonal variability followed the one in the 1-D model (Fig. A1.2). However, the variability patterns in the coastal and open ocean revealed substantial deviations (Fig. 7) reaching 2 °C in the seasonal thermocline. The subsurface maxima of the anomalies demonstrated that the differences

BGD
11, 281–336, 2014

were rather a consequence of the dynamics and not of the local atmospheric forcing. On the overall, the coastal zone was cooler than the open ocean.

4.3 The Black Sea biogeochemistry as seen in isopycnic coordinates

It was explained in the Introduction that the oxygen and hydrogen sulfide dynamics is in the focus of the biogeochemistry analyses of present study. In the following a "mix" of data from observations and numerical modelling is first presented as an initial step to understanding the spatial distribution of oxygen and hydrogen sulfide. The 3-D model provided the density field (see for example the zonal cross-section of density in Fig. 6c and d). The mean profile from Fig. 3 was then used to map the oxygen concentrations as a function of density onto geometric space for the same days (Fig. 8). Obviously, the patterns of the two fields (density and oxygen) are similar; the oxygen isoline 50 µM follows the isopycnic surface 1015 $kg\,m^3$ (compare with Fig. 6). The isoline 5 µM, to which we refer as to the middle of the suboxic zone (or a boundary between suboxidized and subreduced zones, where the oxygen concentrations are close to the detection limit of 3 µM), descended to about 160 m in the coastal regions and ascended to about 100 m in the basin interior. The above considerations hold approximately if we have chosen the isoline 10 or 15 µM, that is the upper boundary of the suboxic zone, because this layer is very thin (see Appendix A and next section).

The horizontal distribution of oxygen at 80 m (Fig. 8c and d) displayed the shape of pycnocline. The minimum of oxygen was observed in the central parts of the Black Sea, which was due to the basin-scale upwelling, the maxima along the coast were due to the coastal circulation bringing oxygen-rich water into the deeper layers. The wide zone of oxygen maximum west of the Crimea (Fig. 8c) was associated with the intense quasi-permanent Sebastopol eddy in this region. The following part of the paper aims at demonstrating that the 3-D modelling approach makes a substantial step ahead in comparison with this simplified approach to reconstruct the 3-D oxygen field. Said in other words we will identify what the numerical simulations add to the results presented above.

BGD
11, 281–336, 2014

The hypothesis of tracer's alignment along the pycnocline gave an additional justification of the relatively simple boundary condition at 200 m used in the numerical model. The formulation of this boundary condition used mapping of one profile in density coordinates onto geometric space and time provided the density distribution from the numerical model was known at any location and time.

5 Model validation

5.1 The mesoscale dynamics as seen in the data from argo profiling floats

Two Argo floats were deployed on 7 May 2010 in the northern Black Sea. The floats known as the Navigating European Marine Observer (NEMO) profilers were equipped with temperature, salinity and oxygen sensors. The sensor for temperature and salinity was CTD SBE 41, and the one for oxygen was Anderaa Oxygen Optode 3830. The trajectories of the two floats (NEMO-0144 & NEMO-0145) were shown in Fig. 1. Their initial positions were close to each other, but they departed one from another soon after the deployment. The float NEMO-0144 entered the central basin and ceased operations on 28 December 2012; the other one NEMO-0145 moved along the western and southern coasts and continued operations until 27 November 2012. Both floats were programmed to sample the water column from the sea surface down to 500 m and transmit the data every 5 days via satellite. More details on the deployment, assessment of the data quality and their analysis was given by Stanev et al. (2013).

This deployment enabled for the first time more than two years-long continuous observations in the Black Sea (Fig. 9). The fact that the two floats operated in two dynamically very different areas, the open ocean and the coastal zone, gave the unique opportunity to compare synchronously the differences between changes of hydrochemistry in these different zones. From the NEMO-0144 float only the data, which were representative of Open Ocean were presented in Fig. 9 that is the data which were measured after 6 July 2010 when the float entered the deep sea. It is noteworthy the subsurface

BGD
11, 281–336, 2014

maximum of oxygen at about 25 m. The oxygen isoline 5 µM and 50 µM were very close one to another, which gave an idea about the thickness of transition zone at the upper boundary of suboxic zone. The depth of suboxic zone as identified from the depth of 5 µM oxygen surface showed relatively small ranges (50–90 m in the open ocean). The CIL (dark blue colored in Fig. 9c and d) was clearly observed in the records of both floats. Salinity in the open ocean was changing very little and in a smooth way (compare Fig. 9e and f).

The coastal float NEMO-0145 revealed vigorous changes of oxygen manifesting the importance of the mesoscale processes for the oxygen change. The oxygen isoline of 5 µM penetrated down to 170 m in February 2012. During this time the float was north of the Minor Asia coast. The short duration of this change and the correlation with similar changes in temperature and salinity makes the coastal eddies the most plausible candidates to explain this event. The isoline of 50 µM was recorded much deeper than in the open ocean, which indicated that the oxygen distribution was a function of the general circulation characterized by an upward motion in the basin interior and sinking in the areas of coastal anticyclones (see also the description of the circulation in Sect. 4).

The correlation between time vs. depth oxygen and salinity diagrams (compare with Fig. 9a and b and 9e and f) demonstrated that mesoscale eddies contributed largely to the variations of oxygen (the increase of oxygen occurred at the time when salinity decreased). However, for some events (e.g., the one seen by NEMO-0144 in November 2011), there was almost no "counterpart event" in the halocline depth, revealing that the hydrochemistry processes do not always follow the evolution of the physical system.

The isolines in Fig. 9c and d display the formation and evolution of the CIL. This layer was refilled every year in February–March. The variations in the depth of its lower boundary, which were very pronounced in the coastal zone, correlated with the oscillations of the depth of the pycnocline. The thickness of CIL increased dramatically

BGD
11, 281–336, 2014

in February 2012, which was caused by the extremely cold winter, and this situation persisted along the southern coast until December 2012.

The CIL in the central basin was thinner than in the coastal zone reflecting the impact of upwelling and downwelling, respectively. The range of mesoscale variability in the central basin was very low. As explained by Stanev et al. (2013) who used data from all available floats in the Black Sea, the temperatures of the CIL observed in the last decade was warmer than 8 °C (see Blatov et al., 1984 for the definition of CIL), which suggests revisiting the accepted definition.

5.2 Comparison between the numerical simulations and observations

The observations and 3-D simulations follow the known from the 1-D simulations temporal variability in the vertical profiles (see Fig. 7 of He et al., 2012 and Fig. A2). In both data sets the mean oxygen values in the coastal zone were higher than in the open ocean. The observed standard deviation of oxygen from the mean oxygen profiles (NEMO-0144 and NEMO-0145) and the numerically simulated standard deviation displayed in Fig. 10 demonstrated that the simulated pattern of temporal variability replicated relatively well the observed one; the magnitudes of the maxima were also similar. The oxygen stratification was stronger than in the observations; the shallower penetration of oxygen signal in the coastal zone in comparison to the observations can be explained by the lower intensity of coastal (anticyclonic) circulation simulated in the model. This calls for using in the future simulations finer horizontal resolution (full eddy resolution) and not only eddy permitting resolution as used here.

The temporal variability of the upper layer oxygen can be well illustrated with the help of the oxygen vs. temperature relationships (Fig. 11). These profiles were characterized by almost vertical curves in the late fall and beginning of winter, that is with a relatively homogeneous oxygen distribution in the cold season. The lowest oxygen values at sea surface approached in summer 250 µM both in the model and observations. The warming of surface waters was accompanied with a decrease in the surface-oxygen concentration and the formation of oxygen subsurface maximum (see also Fig. 9a and b). One

BGD
11, 281–336, 2014

could expect that this oxygen maximum was the analogue of the CIL (e.g., oxygen-rich water overlain in summer by less oxygenated water). However, it is noteworthy that the core of this layer was higher than the core of the CIL (compare Fig. 9a and b and Fig. 9c and d). Furthermore, a closer analysis of observations demonstrated that some summer values in the core of the oxygen maximum were higher than the ones in winter. This excluded the possibility that subsurface oxygen maximum was just a direct result of oxygen-rich water created by winter convection and remained overlain in summer by low oxygen surface water (because of the high SST). The observed absolute oxygen maximum in the subsurface layers was consistent with the findings of Yakushev et al. (2007), Konovalov et al. (2006) and Gregoire and Soetart (2010) who claimed that 71 % of the oxygen in the Black Sea was due to phytoplankton, which shows larger production in summer.

The conclusion from this comparison between numerical simulations and observations is that the model was able to replicate almost all observed features of oxygen dynamics, which made it a useful tool to investigate the upper-ocean hydrochemistry of Black Sea.

6 Temporal and spatial variability of the upper-ocean hydrochemistry

6.1 Seasonal variability

The temporal evolution of simulated oxygen and hydrogen-sulfide (Fig. 12a) replicated the basic features observed by the Argo floats: formation of oxygen rich surface water in winter associated with the convection of cold water (the vertical isolines are due to convective mixing), subsurface oxygen maximum persisting in the warm part of the year, as well as pronounced shorter-term variability. The weakening of the oxygen maximum in summer and fall demonstrated that oxygen was rapidly consumed in the process of oxidation of organic matter (mainly) and reduced species (Sorokin, 2002; Yakushev et al., 2007) during the re-stratification period.

BGD
11, 281–336, 2014

The temporal variability of the suboxic zone followed the one of the salinity (deepening of oxic water was observed where halocline deepened). This was consistent with the observations and supported the idea that the alignment of H_2S to density surfaces (see Fig. 3) was the first-order process governing the distribution of H_2S. Furthermore, the coupled model appeared consistent with earlier simulations of Oguz et al. (2001a), Yakushev et al. (2007), Gregoire et al. (2008) as this concerned the rest of model variables. Nitrate maximum was persistently observed in the analysed location at about 80 m (not shown here). In the deeper layers the temporal variability of ammonium followed the one of the salinity.

Manganese cycling, in which the dissolved manganese was oxidized to produced particulate manganese was known to play an important role in the formation of suboxic zone (Yakushev, 1998; Debolskaya and Yakushev, 2002; Belyaev et al., 1997; Oguz et al., 2001a). In the simulations the maximum of particulate manganese appeared only where the concentrations of oxygen and sulfide were very low (Fig. 12b). Both nitrates and Mn^{4+} layers ascend to the ocean surface in winter as a result of the vertical mixing caused by the winter convection. Mn^{4+} layer was very thin, which agreed with the observations made during *Knorr* 2001 survey and numerical simulations of Yakushev et al. (2009). In addition to what has been known before, this layer revealed a vigorous short-term variability. This temporal and spatial variability did not fully follow the one of oxygen and sulfide identifying active biogeochemical interactions. This proves that the biogeochemistry variability was not only a response to synoptic or mesoscale variability in the circulation, but underwent its own natural evolution.

Although the 3-D oxygen dynamics in the Black Sea has been widely addresses by Grégoire et al. (1998), Grégoire and Lacroix (2001), and Oguz and Salihoglu (2000), the diapycnal aspects of the problem are still not sufficiently described. The comparison between the 1-D model simulations and the basin mean 3-D simulations (Fig. 13) demonstrated some important differences: (1) the oxygenated upper layer in the 1-D simulations was thinner than in the 3-D simulations, (2) the vertical gradients were

BGD
11, 281–336, 2014

stronger in the 1-D simulations; (3) the suboxic zone was deeper and thicker in 3-D simulations.

The overall result of the comparison between simulations from 1-D and 3-D models was that the basin-mean vertical column in the former showed weaker variations. Although the same boundary conditions were used in the two models, the oxic zone was deeper in the 3-D simulations, demonstrating clearly the role of circulation for establishing the vertical stratification of hydrochemistry fields. We remind here that the relatively smooth behaviour of the seasonal signal in Fig. 13b was rather a consequence of the basin averaging. The comparison between deep and coastal ocean fields (see further discussion in the paper) revealed that the winter cooling reached larger depths in the coastal ocean and the anoxic layer was strongly eroded there by the sinking oxygen-rich water. In the 1-D model (without spatial dynamics) the temporal variability of anoxic waters was very low.

It became obvious that the most unrealistic drawback of the 1-D simulations, which was the very thin suboxic zone, has been substantially corrected in the 3-D simulation. This resulted in a better agreement of the numerical simulations with the observations. The suboxic zone in the 3-D simulation was thinner in spring and thicker in summer, while its thickness almost did not change in the 1-D simulation (Fig. 13). These differences between the 1-D and 3-D simulations were interpreted as a consequence of the circulation.

The representation of the same signals in isopycnal coordinates gave a clearer idea about the major sources of the variability in the upper-ocean oxygen content. The low surface density values disappeared in winter and an outcropping of density surfaces down to $\sigma_t = 14.2$ were simulated on 15 February. This was accompanied by an injection of oxygen-rich water into the pycnocline during winter, as seen in the basin-averaged conditions. The secondary subsurface maximum appearing above the major one (at about $\sigma_t = 14$) was replicating a similar maximum observed by the profiling floats in the upper seasonal thermocline (see Fig. 9). As said earlier, this enhancement of the subsurface oxygen maximum could be explained by the role of biological

BGD
11, 281–336, 2014

processes (Yakushev et al., 2007; Konovalov et al., 2006; Gregoire and Soetart, 2010) which were responsible for the O_2 production by phytoplankton. Without this process the core of the oxygen-rich surface water would constantly diffuse in time before the next convective event. This was actually the case for temperature, for which there were not internal sources. Actually, the inflow from the Bosporus Straits tended to increase the temperature in deep layers, however, this signal penetrated much deeper than the processes concerned here.

As conclusion, the major difference between the 1-D and 3-D simulations was that in the 3-D simulations the main subsurface oxygen maximum appeared in a narrower σ_t interval (Fig. 13).

6.2 Spatial variability

6.2.1 Analysis along vertical sections

In the upper mixed layer the basic oxygen patterns in winter were characterized by the surface maximum and a very sharp oxygen-stratification at 50 m marking the depth of direct ventilation from the sea-surface (Fig. 14a). The deepening of the oxygen isoline 5 µM, describing approximately the position of the upper boundary of suboxic zone, down to about 100 m in winter along the western and eastern coasts presented an important evidence of coastal-water ventilation. This surface remained almost horizontal at around 80 m (Fig. 14a and b) in the basin interior. In summer the surface oxygen values dropped to about 250 µM, which was consistent with the observations from profiling floats (see Figs. 9 and 11). The subsurface oxygen maximum covered in summer the entire deep part of the Black Sea with its core at about 30 m (Fig. 14b).

While the area of coastal downwelling was well revealed in the simulations by the deepening of the oxygenated waters in the coastal zone of the western basin (Fig. 14a), this situation was not always the case, as seen in the summer cross-section (Fig. 14b). Furthermore, the thickness of the suboxic zone (here presented as the space between oxygen and sulfide isolines 5 µM) increased in summer. Its lower boundary deepened

BGD
11, 281–336, 2014

from 100 m in February to about 140 m in July. This change was associated with the decrease of density stratification in summer, the density isoline of 16 $kg\,m^{-3}$ was at about 125 m in February and 155 m in July. Furthermore, the sinking Mn^{4+} layer (93 m in February and 120 m in July) was another important process associated with the summer deepening of the lower boundary of suboxic zone.

Under the assumption that standard (linear) tracer–density relationships were valid basin-wide (see Sect. 4.3), the vertical sections in density coordinates (Fig. 14c and d) would show a horizontal (in density space) isolines of oxygen and sulfide. Obviously, this was not the case in the simulations and these figures gave an idea about the isopycnal mixing. The isolines of both variables almost mirrored the density plots in Fig. 5c and d which could illustrate that in the areas of shallower depth of isopycnic surfaces the oxygen concentrations would be larger because the shallower position is closer to sea surface where the oxygen content is larger. On the opposite, the deeper position of isopycnic surface would tend to decrease the concentration of oxygen because in the deeper layers the consumption of oxygen would be larger. The agreement between oxygen distribution and density is particularly well seen in winter above the suboxic zone (σ_t = 14.5–15). In summer the along-isopycnal contrasts are smaller, which reflects the lower intensity of the summer circulation. During this season the lower boundary of suboxic zone (H_2S = 5 µM) mirrored better the shape of density surfaces (in particular for the levels below σ_t = 14.5) than the oxygen isolines the layers above did.

The above results motivated us to analyze the differences between stratification in particular time and along particular section and the basin mean one (Fig. 15). This difference would "remove" the mean situation known from the 1-D modeling and make clearer the contribution of the 3-D dynamics. The "anomaly"-representation makes the origin of surface oxygen-rich water (largest positive anomalies in winter) very clear. Not quite trivial was the negative anomaly originating from the sea surface, which gave an indication of localized convection. In these "chimneys" (e.g. Fig. 15a) the vertical

BGD
11, 281–336, 2014

mixing resulted in a consumption of oxygen by sulfide (through the other elements intermediates), leading to lower oxygen values.

The anomaly-plots in winter revealed several thinner zones localized around the areas where the pycnocline was in its highest position. In these areas the upward motions changed the stratification with respect to the mean one resulting in the formation of multi-layer vertical structure of oxygen anomaly. In summer, the oxygen anomaly at the same section was represented by the following: (1) a negative anomaly in the coastal zone (Fig. 15c and d), (2) oxygen anomaly following the main pycnocline represented by the thin blue strip, and (3) thin secondary maxima and minima in the upper 50 m layer. Obviously, the horizontal anomalies from the mean (Fig. 15a and c) correlate well with the shape of pycnocline (Fig. 6c and d). The diapycnal mixing in the area of multiple layers is supposed to act as the major agent controlling the matter exchange. This is justified by the presentation of the same cross-sections in isopycnic coordinates (Fig. 15e–h). The intermediate layers of positive anomaly at about σ_t = 15 (Fig. 15e and f) provided the major source for isopycnal mixing. From the upwelling zones, the oxygen-rich waters propagated in the direction of down-welling zones that is the coastal zone, as well as to the basin interior the latter separating the western and eastern gyres. As a conclusion of the above discussion (mostly focused on the winter situation) one could summarize that the outcropping appeared to be the major mechanism pumping oxygen-rich water into the pycnocline. The upwelling gave the second mechanism to increase oxygen concentrations. Double cells were formed (one in each gyre). Propagating approximately along the doomed isopycnal surfaces these waters tended to distribute basin-wide the positive oxygen anomalies.

In summer the oxygen anomalies were overall positive in the eastern basin where a two-layer structure was developed (Fig. 15g). Along the north–south section (Fig. 15h) a clear indication of developed suboxia existed. This area served as an oxic sink for relatively large areas in the western basin. The slope area acted as a guide for the diapycnal mixing in summer forming one branch of the vertical oxygen-conveyor-belt. Furthermore, a number of local anomalies were seen in the area of CIL and below

BGD
11, 281–336, 2014

it. They give a clear evidence of diapycnic mixing in the basin interior as well as the resulting intrusions which follow the neutral surfaces.

6.2.2 Analysis along horizontal sections

The horizontal distribution of oxygen at 50 m (Fig. 16a and c) revealed an important seasonal change consisting in the following: while the coastal maximum in February was observed mostly in the area of northwestern shelf (Fig. 16a), the summer maximum was in the interior part of the western basin (Fig. 16c) and followed along the southern and eastern costs. The pattern of oxygen-rich waters at 50 m in winter was explained by the extreme cooling of the western basin and the resulting ventilation. In the same area low-oxygen waters propagated along the continental slope in summer (Fig. 16c) from the area of Crimea Peninsula along the western and part of the southern coasts. The western gyre gave the origin of the oxygen maximum, which reached the area of Kerch strait following the coast (Fig. 16c).

The role of the sub-basin circulation features was better seen at 80 m (Fig. 16e and g). The winter pattern indicated an increased concentration to the southeast of Crimea Peninsula (Fig. 16e), which was caused by the downward propagation of water in the area of Crimean eddy. The downward motions explained the increased oxygen concentrations in most of the coastal area (Fig. 16e), which was well seen around the southern coasts as very thin high-oxygen strips. In the eastern most part of the sea, the Batumi eddy in summer (Fig. 16g) played the role of the oxygen source for the deeper layers.

The distribution of oxygen on selected isopycanl depths (σ_t = 14.5 and σ_t = 15.5) in February (Fig. 16i and m) and July (Fig. 16k and o) revealed the major pathways of the penetration of oxygen into the pycnocline and its consumption. The summer and winter seasons revealed different mechanisms of upper-ocean hydrochemistry. In winter, the outcropping in the basin interior enabled the oxygen to penetrating deeper into the pycnocline (Fig. 15i and m). In this season the overall isopycnal transport (from high to low values) was directed from the ocean interior towards the rim current. Several small-

BGD
11, 281–336, 2014

scale exceptions were noteworthy (the small region south of Crimea and along the western and southern coasts) where the oxygen-rich waters propagated at σ_t = 14.5 from the coast in the direction of Rim Current. This feature did not penetrate deeper (to σ_t = 15.5) as seen in Fig. 16 m. The conclusion from the discussion of the winter situation is that the oxygen patterns adjust to the intense basin dynamics. They can be easily explained based on the known (from modeling or observations) dynamics.

As seen in the comparison between Fig. 16c and g no clear relationship to basin circulation existed in summer. During this season (1) the sea surface could not be considered as an important source of oxygen because of the high summer temperatures, and (2) the Black Sea circulation was much less intense and shaped in a very different way the oxygen patterns. The patterns seen in isopycnic coordinates (Fig. 16k) again revealed a boundary aligned isopycnal mixing (without isopycnal mixing the distribution of O_2 would be horizontally homogeneous). However the process was completely different along the western continental slope (a relatively mild slope) which acted as a sink of oxygen and in the rest of the coastal sea which acted as a source for the isopycnic mixing. However this contrast (coast vs. Open Ocean) changed direction at σ_t = 15.5, demonstrating a complicated vertical structure of isopycnal mixing.

The comparison between the summer and winter cases (e.g. Fig. 16i and k) necessitated to explain the reason of the simulated differences. One step in this direction was to examine the correlation between the patterns in depth and density coordinates. On the overall, the comparison between Fig. 16a and i (winter) revealed a negative correlation, while the comparison between Fig. 16c and k (summer) revealed a positive correlation. This would mean that it is not the intensity of the circulation in summer, which dominated the distribution of oxygen but rather the vertical (diapycnic diffusion) bringing oxygen-rich water from the core of subsurface layer into the pycnocline. The strengthening of coastal anticyclones and the weakening of the general circulation in summer (Staneva et al., 2001) would work in the same direction. Summarizing the comparison between the winter and summer situation it is noteworthy that while the former was dominated by the intense basin-wide circulation and sources at sea sur-

BGD
11, 281–336, 2014

face, the latter was dominated by mesoscale circulation and small-scale mixing. Thus two contrasting regimes dominate isopyclal diffusion in winter and summer: gyre driven in winter and eddy driven in summer.

There is however another important question to ask: is only the hydrodynamics in such a complex biogeochemistry model as ROLM the only important factor shaping the upper-ocean hydrochemistry. This issue deserves a profound separate study. Here only the simulated patterns of phytoplankton below the photic layer will be illustrated. The comparison between Fig. 16a and Fig. 16b revealed the negative correlation between the horizontal patterns of oxygen and phytoplankton in winter in the upper layers (50 m). This situation changed to a positive correlation at about 80 m, which was exemplified by the positive anomalies of both variables in the coastal zone and the intrusion originating from the southern tip of Crimea Peninsula.

While the summer concentrations of oxygen at 50 m was characterized by larger values in most of the coastal zone (Fig. 16c), the distribution of phytoplankton at this depth (Fig. 16d) showed a patchy structures with maxima to the south of the Danube Delta and to the west of the Crimea Peninsula. Obviously, in this part of the year there was no clear correlation in the distribution of oxygen and phytoplankton at 50 m. The same was valid also for the sections at 80 m (compare Fig. 16g and h).

The comparison between the oxygen and phytoplankton patterns in isopycnic coordinates (Fig. 16i and j) during winter revealed another interesting regularity: while the area of oxygen maximum was simulated in the basin interior the maximum of phytoplankton (both patterns show the control of the same dynamics) was shifted into the area of Rim Current. The coastal areas showed low concentrations for both oxygen and phytoplankton. Differently from this (winter) situation the pattern of oxygen and phytoplankton at $\sigma_t = 14.5$ did not agree well in summer. However, deeper (at $\sigma_t = 15.5$) the patterns of the two field were in a very good correlation, compare Fig. 16m and n (winter) and Fig. 16o and p (summer). In conclusion one could summarize that the dynamics of biogeochemistry did not always follow the hydro and thermodynamics, which brought another level of complexity of the considered biogeochemistry system. We re-

BGD
11, 281–336, 2014

mind here that similar conclusion was derived from the analysis of Fig. 12 describing the evolution of Mn^{2+} and Mn^{4+}.

7 Conclusions

In this paper we gave some new insights on the oxygen variability in the Black Sea by means of analysis of historic data, continuous oxygen observation from profiling floats and 3-D numerical model simulations. The temporal evolution of the vertical distribution of oxygen is very different in the coastal and open ocean. The upper boundary of suboxic zone demonstrated much stronger variations in the coastal area than in the deep part of the basin. Numerical simulations with the 3-D physical-biogeochemical coupled numerical model appeared a useful tool supporting the understanding of the spatial and temporal variability of suboxic zone. It was demonstrated that an extremely fine vertical resolution was needed (about 2 m) for the correct simulation biogeochemical process. In order to keep the computational requirements for three-dimensional simulations reasonable the 3-D model was set up for the upper 200 m part of the water column using appropriate boundary conditions.

The numerical model, although set up only for the upper 200 m layer, was able to reproduce the main features of water mass circulation in the Black Sea: the cyclonic circulation and the interior upwelling as well as the coastal anticyclones. This realistic physical background was very basic for the realistic simulations of horizontal and vertical transport and mixing of chemical properties, as well as their temporal-spatial variability. The temporal variability of upper and lower boundaries of suboxic zone showed a clear seasonal character. Further to the study of Stanev et al. (2004) it was demonstrated that pronounced diapycnal mixing dominated not only the Black Sea thermodynamics at the depth of the CIL, but also its biogeochemical state. One of the basic conclusions from this paper was that the hypothesis of property alignment to the isopycnal surfaces depicted very coarsely the oxygen distribution (in particular in the suboxic zone) and that using three-dimensional model was the better choice to enhance the

BGD
11, 281–336, 2014

realism of simulations. Furthermore, the control of dynamics on the Black Sea ecosystem appeared very different for summer and winter (gyre transport vs. mixing dominated controls). Coastal-to-open sea differences revealed strong contrasts enhancing the isopycnic mixing, which appeared quite diverse in different layers, along the steep continental slop or over bottom topography characterized by milder changes. This extreme variety calls for deeper analyses and more focused study on the temporal-spatial variability of individual variables. Some further developments are also needed as for instance using more realistic riverine fluxes, increasing horizontal resolution (moving from eddy permitting to eddy resolving coupled models), giving deeper consideration of light regime and sedimentation. Among the computational challenges is the extension of the model grid down to the bottom (about 2000 m), which could be facilitated by the use of adaptive grids in the vertical.

Appendix A

1-D coupled physical-biogeochemistry model

This Appendix is motivated by the need to discuss the optimal vertical resolution of the model, which has to be consistent with the complex biochemical processes, in particular the ones taking place in the very thin (about 20–30 m) suboxic zone. Three experiments with different vertical resolution were carried out using 1-D coupled General Ocean Turbulence Model (GOTM) and ROLM. The basic model run with a vertical resolution of 2 m (experiment A) was essentially the same as the one described by He et al. (2012). The maximum water depth was 200 m that is 100 model levels were used. Such resolution would be very computationally intensive if used in the 3-D model therefore results of two sensitivity experiments (B and C) with vertical resolution of 5 and 20 m, correspondingly, are first discussed in order to demonstrate the resolution limits.

BGD
11, 281–336, 2014

All experiments used the same initial and boundary conditions and the meteorological forcing was computed using atmospheric data from the ECWMF reanalysis (http://www.ecmwf.int) as it has been explained by He et al. (2012). At the sea surface oxygen flux was computed as in Yakushev et al. (2006, 2007):

$$Q_{O_2} = k_{660} \cdot (Sc/660)^{-0.5} \cdot (O_{2sat} - O_2), \quad \text{(A1)}$$

where O_{2sat} is the oxygen saturation concentration computed as a function of temperature and salinity (UNESCO, 1986), Sc is the Schmidt number for oxygen, k_{660} is the reference gas-exchange transfer velocity computed as $k_{660} = 0.365W^2 + 0.46W$, where W is the wind speed magnitude (Schneider et al., 2002). Fluxes of PO_4 and NO_3 (see Table A1 for the description of variables) were prescribed using the concept developed by Fonselius (1974) who showed that 6700 tons of phosphorus had to be added annually to the Black Sea to balance the deposited bottom phosphorus, ensuring thus that the phosphorus concentration remained at a constant level. The corresponding flux was $Q_{PO_4} = 0.13\,\mathrm{mmol\,m^{-2}\,d^{-1}}$. Using similar considerations, the flux of nutrients due to the rivers input and atmospheric deposition was estimated as $Q_{NO_3} = 1.5\,\mathrm{mmol\,m^{-2}\,d^{-1}}$ (Yakushev et al., 2006).

At the lower model boundaries, the following values of model variables (see Table A1.1 for the abbreviations corresponding to the names of ROLM variables) have been prescribed according to the existing observations: $NH_4 = 20\,\mu M$, $PO_4 = 4.5\,\mu M$, $H_2S = 60\,\mu M$, $Mn^{2+} = 8\,\mu M$, $Fe^{2+} = 0.4\,\mu M$ (in experiments A, B and C). Model parameters are given in He et al. (2012).

The model has been integrated in time until the solution has reached a quasi-periodic state. Four model variables were chosen to analyse the effect of resolution (Fig. A1). At fist glance the major difference between the simulations with different vertical resolution was the coarse resolution of the vertical profiles, in particular in the 20 m resolution case. Not less important, however is that in the simulations with 2 m resolution (experiment A) O_2 and H_2S did not overlap, which was consistent with the concept that the suboxic zone decoupled oxic and anoxic waters. In experiment B, oxygen and sulfide

BGD
11, 281–336, 2014

overlapped slightly, whereas the coexistence of O_2 and H_2S in experiment C at 55–85 m totally disagrees with the observations. The maximum of nitrate (6 µM at about 55 m) was sharper in experiment A, which agreed well with the observations presented by Yakushev et al. (2006). This layer was more "diffuse" in experiment B and badly resolved in experiment C. The present result demonstrated a similarity with the sensitivity experiments of Yakushev et al. (2009), however, while in the later work the abnormally high vertical diffusion was the reason for the disappearance of suboxic zone, the same effect in the present simulation was caused by the coarse vertical resolution. We remind here that with the used model parameters (see He et al., 2012) the simulated suboxic layer was thinner than the one seen in the observations. However, it was not aimed here to improve the performance of 1-D model because, as shown further in the paper, this drawback was rather a consequence of the oversimplifications in the 1-D frame and disappeared in the 3-D model.

The performance of physical model (Fig. A2) revealed the well-known variability in the seasonal thermocline. Cold water, which formed at the sea surface in winter penetrated down to about 100 m, and was overlain in summer by warm surface water. The simulated salinity showed a 50 m thick surface layer with low salinity and strong vertical changes between 70 and 120 m, which was actually the zone of the main pycnocline. Turbulent kinetic energy was very small in summer because of the strong vertical stratification, which shielded deeper layers from the surface processes. This decoupling between upper and deeper layers is of utmost importance for the simulated biogeochemistry processes in the upper ocean.

Acknowledgements. We thank A. Stips for the discussions on the boundary conditions of GETM, and M. Gregoire for the comments on biogeochemistry processes relevant to this paper. A. Boetius and F. Janssen supported the deployment of the Argo floats, R. Kandilarov helped to prepare the model topography. Atmospheric model data were produced by the European Centre for Medium-Range Weather Forecasts (ECMWF). This work was a continuation of the EU-founded HYPOX project. EVS acknowledges support from the EC Grant 312642; JS acknowledges support from the EC Grant 287600.

The service charges for this open access publication have been covered by a Research Centre of the Helmholtz Association.

References

Basturk, O., Saydam, C., Salihoglu, I., Eremeeva, L. V., Konovalov, S. K., Stoyanov, A., Dimitrov, A., Cociasu, A., Dorogan, L., and Altabet, M.: Vertical variations in the principle chemical properties of the Black Sea in the autumn of 1991, J. Marine Chem., 45, 149–165, 1994.

Belyaev, V. I., Sovga, E. E., and Lyubartseva, S. P.: Modelling the hydrogen sulfide zone of the Black Sea. Ecol. Model., 13, 51–59, 1997.

Blatov, A. S., Bulgakov, N. P., Ivanov, V. A., Kosarev, A. N., and Tujilkin, V. S.: Variability of Hydrophysical Fields in the Black Sea, Gidrometeoizdat, Leningrad, 240 pp., 1984 (in Russian).

Buesseler, K., Michaels, A., Siegel, D., and Knap, A.: A three dimensional time-dependent approach to calibrating sediment trap fluxes, Global Biogeochem. Cy., 8, 179–193, 1994.

Burchard, H. and Bolding, K.: GETM – a General Estuarine Transport Model, Scientific Documentation, European Commission, Report EUR 20253, 155 pp., 2002.

Burchard, H., Bolding, K., Villarreal, M. R., Rippeth, T. P., Fisher, N., and Stips, A.: The GOTM modelling system, in: Marine Turbulence: Theories, Observations and Models, edited by: Baumert, H. Z., Simpson, J. H., and Sündermann, J., Cambridge University Press, Cambridge, 213–224, 213–224, 2005.

Capet, A., Beckers, J.-M., and Grégoire, M.: Drivers, mechanisms and long-term variability of seasonal hypoxia on the Black Sea northwestern shelf – is there any recovery after eutrophication?, Biogeosciences, 10, 3943–3962, doi:10.5194/bg-10-3943-2013, 2013.

Debolskaya, E. I. and Yakushev, E. V.: The role of suspended manganese in hydrogen sulfide oxidation in the Black Sea redox-zone, Water Resour., 29, 72–77, 2002.

Deuser, W. G.: Evolution of anoxic of anoxic conditions in the Black Sea during Holocene, The Black Sea-Geology, Chemistry and Biology, 2, 133–136, 1974.

Fonselius, S. H.: Phosphorus in the Black Sea, in: The Black Sea – Geology, Chemistry and Biology, edited by: Degens, E. J. and Koss, D. A., Amer. Ass. of Petrol. Geologists, Tusla, 144–150, 1974.

BGD
11, 281–336, 2014

Grayek, S., Stanev, E. V., and Kandilarov, R.: On the response of Black Sea level to external forcing: altimeter data and numerical modelling, Ocean Dynam., 60, 123–140, 2010.
Grayek, S., Staneva, J., Schulz-Stellenfleth, J., Peterson, W., and Stanev, E. V.: Use of FerryBox surface temperature and salinity measurements to improve model based state estimates for the German Bight, J. Marine Syst., 88, 45–59, 2011.
Gregg, C. M., Ozsoy, E., and Latif, M. A.: Quasi-steady exchange flow in the Bosphorus, Geophys. Res. Lett., 26, 83–86, 1999.
Gregg, M. C. and Yakushev, E.: Surface ventilation of the Black Sea's cold intermediate layer in the middle of the western gyre, Geophys. Res. Lett., 32, L03604, doi:10.1029/2004GL021580, 2005.
Grégoire, M. and Lacroix, G.: Study of the oxygen budget of the Black Sea waters using a 3D coupled hydrodynamical-biogeochemical model, J. Marine Syst., 31, 175–202, 2001.
Grégoire, M. and Lacroix, G.: Exchange processes and nitrogen cycling on the shelf and continental slope of the Black Sea basin, Global Biogeochem. Cy., 17, 1073, doi:10.1029/2002GB001882, 2003.
Grégoire, M. and Soetaert, K. E. R.: Carbon, nitrogen, oxygen and sulfide budgets in the Black Sea: a biogeochemical model of the whole water column coupling the oxic and anoxic parts, Ecol. Model., 221, 2287–2301, 2010.
Grégoire, M., Beckers, J. M., Nihoul, J. C. J., and Stanev, E.: Coupled hydrodynamic ecosystem model of the Black Sea at basin scale, in: Sensitivity to Change: Black Sea, Baltic Sea and North Sea, edited by: Ozsoy, E. and Mikaelyan, A., NATO ASI Series, Vol. 27, Kluwer Academic Publishers, 487–499, 1997.
Grégoire, M., Beckers, J. M., Nihoul, J. C. J., and Stanev, E.: Reconnaissance of the main Black Sea's ecohydrodynamics by means of a 3D interdisciplinary model, J. Marine Syst., 16, 85–106, 1998.
Grégoire, M., Raick, C., and Soetaert, K.: Numerical modeling of the deep Black Sea ecosystem functioning during the late 80's (eutrophication phase) Prog. Oceanogr., 76, 3, 286–333, 2008.
He, Y., Stanev, E., Yakushev, E., and Staneva, J.: Black Sea biogeochemistry: response to decadal atmospheric variability during 1960–2000 inferred from numerical modeling, Mar. Environ. Res., 77, 90–102, 2012.
Jørgensen, B. B., Fossing, H., Wirsen, C. O., and Jannasch, H. W.: Sulfide oxidation in the anoxic Black Sea chemocline, Deep-Sea Res., 38, S1083–S1104, 1991.

BGD
11, 281–336, 2014

Konovalov, S. K. and Murray, J. W.: Variations in the chemistry of the Black Sea on a time scales of decades (1960–1995), J. Marine Syst., 31, 217–243, 2001.
Konovalov, S. K., Murray, J., and Luther III, G. W.: Basic processes of Black Sea biogeochemistry, Oceanography, 18, 24–35, 2005.
Konovalov, S., Murray, J., Luther, G., and Tebo, B.: Processes controlling the redox budget for the oxic/anoxic water column of the black sea, Deep-Sea Res. Pt. II, 53, 1817–1841, 2006.
Korotaev, G. K., Oguz, T., Dorofeyev, V. L., Demyshev, S. G., Kubryakov, A. I., and Ratner, Yu. B.: Development of Black Sea nowcasting and forecasting system, Ocean Sci., 7, 629–649, doi:10.5194/os-7-629-2011, 2011.
Kuypers, M. M. M., Sliekers, A. O., Lavik, G., Scmid, M., Jorgensen, B. B., Kuenen, J. G., Sinnenghe Damste, J. S., Strous, M., and Jetten, M. S. M.: Anaerobic ammonium oxidation by anammox bacteria in the Black Sea, Nature, 422, 608–611, 2003.
Lancelot, C. L., Staneva, J. V., Van Eeckhout, D., Beckers, J.-M., and Stanev, E. V.: Modelling the Danube-influenced north-western continental shelf of the Black Sea. II: Ecosystem response to changes in nutrient delivery by the Danube River after its damming in 1972, Estuar. Coast. Shelf S., 54, 473–499, 2002.
McDougall, T. J.: The relative roles of diapycnal and isopycnal mixing on subsurface water mass conversion, J. Phys. Oceanogr., 14, 1577–1589, 1984.
Murray, J. W., Jannasch, H. W., Honjo, S., Anderson, R. F., Reeburgh, W. S., Top, Z., Friederich, G. E., Codispoti, L. A., and Izdar, E.: Unexpected changes in the oxic/anoxic interface in the Black Sea, Nature, 338, 411–413, 1989.
Murray, J. M., Codispoti, L. A., and Friederich, G. E.: Oxidiation–reduction encironments: the suboxic zone in the Black Sea, in: Aquatic Chemistry: Interfacial and Interspecies Process, edited by: Huang, C. P., O'Melia, C. R., and Morgan, J. J., Adv. Chem. Ser., No. 224, 1995.
Murray, J. W., Lee, B.-S., Bullister, J., and Luther III, G. W.: The suboxic zone of the Black Sea, in: Environmental Degradation of the Black Sea: Challenges and Remedies, edited by: Besiktepe, S., Unluata, U., and Bologa, A., NATO ASI Series 2, 75–92, 1999.
Neretin, L. N., Volkov, I. I., Bottcher, M. E., and Grinenko, V. A.: A sulfur budget for the Black Sea anoxic zone, Deep-Sea Res. Pt. I, 48, 2569–2593, 2001.
Oguz, T.: The role of physical processes controlling the Oxycline and Suboxic Layer structures in the Black Sea. Global Biogeochem. Cy., 16, 101029–101042, 2002.

BGD
11, 281–336, 2014

Oguz, T., Ducklow, H., Malanotte-Rizzoli, P., Tugrul, S., Nezlin, N., and Unluata, U.: Simulation of annual plankton productivity cycle in the Black Sea by a one-dimensional physical-biological model, J. Geophys. Res., 101, 16585–16599, 1996.

Oguz, T., Ivanov, L. I., and Besiktepe, S.: Circulation and hydrographic characteristics of the Black Sea, in: The Sea, vol. 14, edited by: Robinson, A. R. and Brink, K. H., Harvard University Press, chap. 33, 1331–1369, 1998.

Oguz, T., Ducklow, H. W., and Malanotte-Rizzoli, P.: Modeling distinct vertical biogeochemical structure of the Black Sea: dynamical coupling of the oxic, suboxic and anoxic layers, Global Biogeochem. Cy., 14, 1331–1352, 2000.

Oguz, T., Murray, J. W., and Callahan, A.: Modeling redox cycling across the suboxic–anoxic interface zone in the Black Sea, Deep-Sea Res. Pt. I, 48, 761–787, 2001.

Oguz, T., Malanotte-Rizzoli, P., Ducklow, H. W., and Murray, J. W.: Interdisciplinary studies integrating the Black Sea biogeochemistry and circulation dynamics, Oceanography, 15, 4–11, 2002.

Oguz, T., Tugrul, S., Kideys, A. E., Ediger, V., and Kubilay, N.: Physical and biogeochemical characteristics of the Black Sea, in: The Sea, vol. 14, chap. 33, 1331–1369, 2005.

Peña, M. A., Katsev, S., Oguz, T., and Gilbert, D.: Modeling dissolved oxygen dynamics and hypoxia, Biogeosciences, 7, 933–957, doi:10.5194/bg-7-933-2010, 2010.

Peneva, E. L. and Stips, A. K.: Numerical simulations of Black Sea and adjoined Azov Sea, forced with climatological and meteorological reanalysis data, Technical report, EUR21504EN, European Commission, Ispra, 2005.

Rozanov, A. G.: Redox stratification of the Black Sea water, Oceanography, 35, 544–549, 1995.

Saydam, C., Tugrul, S., Baturk, O., and Oguz, T.: Identification of the oxic/anoxic interface by isopycnal surfaces in the Black Sea, Deep-Sea Res., 40, 1405–1412, 1993.

Schneider, B., Bausch, G., Kubsch, H., and Peterson, I.: Accumulation of total CO_2 during stagnation in the Baltic deep water and its relationship to nutrient and oxygen concentrations, Mar. Chem., 77, 277–291, 2002.

Shaffer, G.: Phosphorus pumps and shuttles in the Black Sea, Letters to Nature, 321, 515–517, 1986.

Skopintsev, B. A.: Formirovanie Sovremennogo Himicheskogo Sostava vod Chernogo Morya (Evolution of the Black Sea Chemical Structure), Gidrometeoizdat, Leningrad, 336 pp., 1975.

Sorokin, Y. I.: Chernoe More: Priroda i Resursi (The Black Sea: the Nature and the Resources), Nauka, Moscow, 217 pp., 1982.

BGD
11, 281–336, 2014

Stanev, E. V.: Numerical modelling of the circulation and the hydrogen sulfide and oxygen distribution in the Black Sea, Deep-Sea Res., 36, 1053–1065, 1989.
Stanev, E. V.: Understanding Black Sea dynamics: overview of recent numerical modelling, Oceanography, 18, 56–75, 2005.
Stanev, E. V. and Kandilarov, R.: Sediment dynamics in the Black Sea: numerical modelling and remote sensing observations, Ocean Dynam., 62, 533–553, 2012.
Stanev, E. V., Simeonov, J. A., and Peneva, E. L.: Ventilation of Black Sea pycnocline by the Mediterranean plume, J. Marine Syst., 31, 77–97, 2001.
Stanev, E. V., Bowman, M. J., Peneva, E. L., and Staneva, J. V.: Control of Black Sea intermediate water mass formation by dynamics and topography: comparison of numerical simulations, surveys and satellite data, J. Mar. Res., 61, 59–99, 2003.
Stanev, E. V., Staneva, J., Bullister, J. L., and Murray, J. W.: Ventilation of the Black Sea pycnocline. parameterization of convection, numerical simulations and validations against observed chlorofluorocarbon data, Deep-Sea Res., 51, 2137–2169, 2004.
Stanev, E. V., He, Y., Grayek, S., and Boetius, A.: Oxygen dynamics in the Black Sea as seen by Argo profiling floats, Geophys. Res. Lett., 40, 3085–3090, doi:10.1002/grl.50606, 2013.
Staneva, J. V., Stanev, E. V., and Oguz, T.: The impact of atmospheric forcing and water column stratification on the yearly plankton cycle, in: Ecosystem Modelling as a Management Tool for the Black Sea, vol. 2, edited by: Ivanov, L. and Oguz, T., Kluwer Academic Publishers, 301–322, 1998.
UNESCO: Progress on oceanographic tables and standards 1983–1986: work and recommendations of the UNESCO/SCOR/ICES/IAPSO Joint Panel, UNESCO Technical papers in Marine Science, 50, UNESCO, Paris, 59 pp., 1986.
Vinogradov, M. E. and Nalbandov, Y. P.: Dependence of physical, chemical and biological parameters in pelagic ecosystem of the Black Sea upon the water density, Oceanology, 30, 769–777, 1990.
Yakushev, E. V.: Numerical modeling of transformation of nitrogen compounds in the redox zone of the Black Sea, Oceanology, 32 173–177, 1992.
Yakushev, E. V.: Mathematical modeling modeling of oxygen, nitrogen, sulfur and manganese cycling in the Black Sea, in: Ecosystem Modeling as a Management Tool for the Black Sea, vol. 2, edited by: Ivanov, L. and Oguz, T., NATO ASI Series, 2-Environmental Security-47, Kluwer Academic Publishers, 373–384, 1998.

BGD
11, 281–336, 2014

Yakushev, E. V. and Neretin, L. N.: One-dimensional modeling of nitrogen and sulfur cycles in the aphotic zones of the Black and Arabian Seas, Global Biogeochem. Cy., 11, 401–414, 1997.

Yakushev, E. V. and Newton, A.: Introduction. Redox interfaces in marine waters, in: Chemical Structure of Pelagic Redox Interfaces: Observation and Modeling, edited by: Yakushev, E. V., Springer, Berlin, Heidelberg, Hdb. Env. Chem., 22, 1–12, doi:10.1007/698_2012_167, 2013.

Yakushev, E. V., Neretin, L. N., and Volkov, I. I.: Mathematical modeling of the transformation of inorganic sulfur compounds in the Redox zone of the Black Sea, Oceanology, 32, 718–723, 1992.

Yakushev, E. V., Pollehene, F., Jost, G., Kuznetsov, I., Schneider, B., and Umlauf, L.: Redox Layer Model (ROLM): a tool for analysis of the water column oxic/anoxic interface processes, Marine Science Reports, No. 68, 2006.

Yakushev, E. V., Pollehne, F., Jost, G., Kuznetsov, I., Schneider, B., and Umlauf, L.: Analysis of the water column oxic/anoxic interface in the Black and Baltic seas with a numerical model, Mar. Chem., 107, 388–410, 2007.

Yakushev, E. V., Chasovnikov, V. K., Murray, J. W., Pakhomova, S. V., Podymov, O. I., and Stunzhas, P. A.: Vertical hydrochemical structure of the Black Sea, in: The Black Sea Environment, edited by: Kostyanoy, A. G. and Kosarev, A. N., The Handbook of Environmental Chemistry, vol. 5, Springer, Berlin, 277–307, 2008.

Yakushev, E., Pakhomova, S., Sørenson K., and Jens, S.: Importance of the different manganese species in the formation of water column redox zones: observations and modelling, Mar. Chem., 117, 59–70, 2009.

BGD
11, 281–336, 2014

Table A1. State variables and their abbreviations used in the text.

Variable	Abbreviation
Dissolved Oxygen	O_2
Hydrogen Sulfide	H_2S
Elemental Sulfur	S^0
Thiosulfate	S_2O_3
Sulfate	SO_4
Ammonia	NH_4
Nitrite	NO_2
Nitrate	NO_3
Particulate Organic Nitrogen	PON
Dissolved Organic Nitrogen	DON
Phosphate	PO_4
Particulate Organic Phosphorus	POP
Dissolved Organic Phosphorus	DOP
Bivalent Manganese	Mn^{2+}
Trivalent Manganese	Mn^{3+}
Quadrivalent Manganese	Mn^{4+}
Bivalent Iron	Fe^{2+}
Trivalent Iron	Fe^{3+}
Phytoplankton	Phy
Zooplankton	Zoo
Aerobic Heterotrophic Bacteria	Bhe (Ox. Het)
Aerobic Autotrophic Bacteria	Bae (Ox. Aut)
Anaerobic Heterotrophic Bacteria	Bha (Anox. Het)
Anaerobic Autotrophic Bacteria	Baa (Anox. Aut)

BGD
11, 281–336, 2014

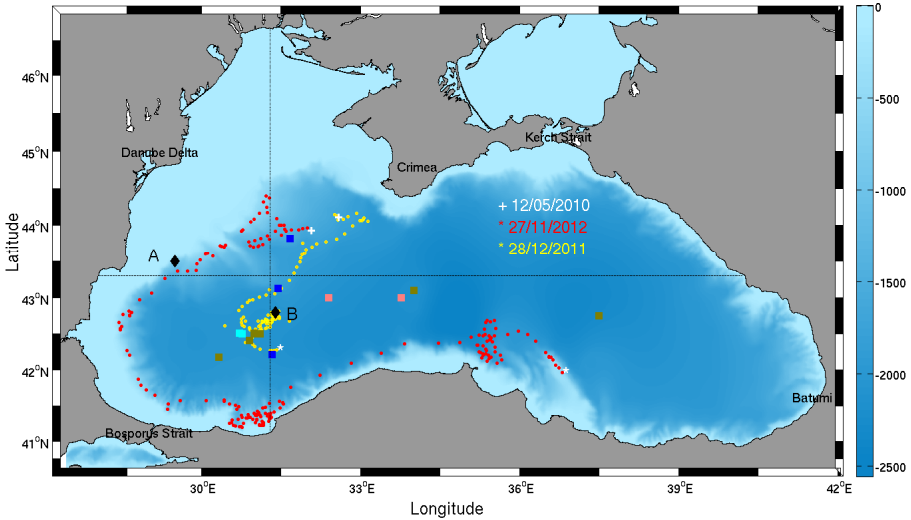

Fig. 1. Black Sea topography. The colour bar indicates ocean depths in meters. Color squares are sites of historical surveys during which oxygen and hydrogen sulfide data have been collected: RV *Lomonsov*, 1964.08 (red), *Atlantis*, 1969.04 (blue), *Knorr*, 2001.06 (cyan), *Knorr*, 2003.05 (brown). Locations of Argo floats surfacing are shown with yellow dots (NEMO-0144) and red dots (NEMO-0145). Deployment position are marked by crosses, the last positions are labelled by stars. Two black diamond symbols (A & B) give the positions where profile data from the 3-D model simulations have been analysed. Analyses of simulations have been also done along the zonal and meridional section lines.

BGD
11, 281–336, 2014

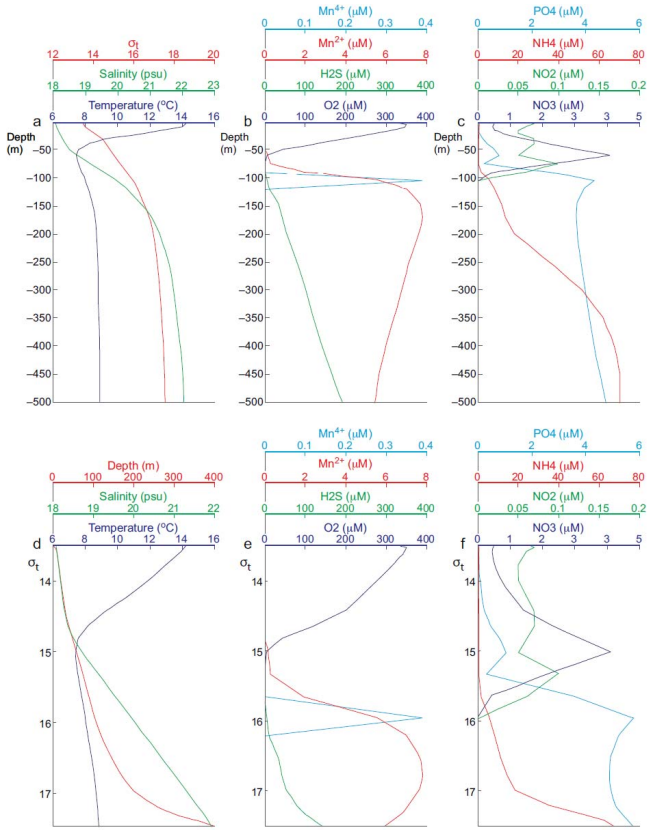

Fig. 2. Vertical profiles of temperature, salinity and σ_t, **(a)**, oxygen, hydrogen sulphide, Mn^{2+} and Mn^{+4} **(b)**, and NO_3, NO_2, NH_4 and PO_4 **(c)** presented in depth coordinates in the upper 500 m. **(d–f)** is the same presented in density coordinates, along with the depth of σ_t levels in **(a)**. The data are from Station St. 231 sampled by RV "*Akvanavt*" cruise 20 in the Eastern Gyre of the Black Sea, 3 December 2000.

BGD
11, 281–336, 2014

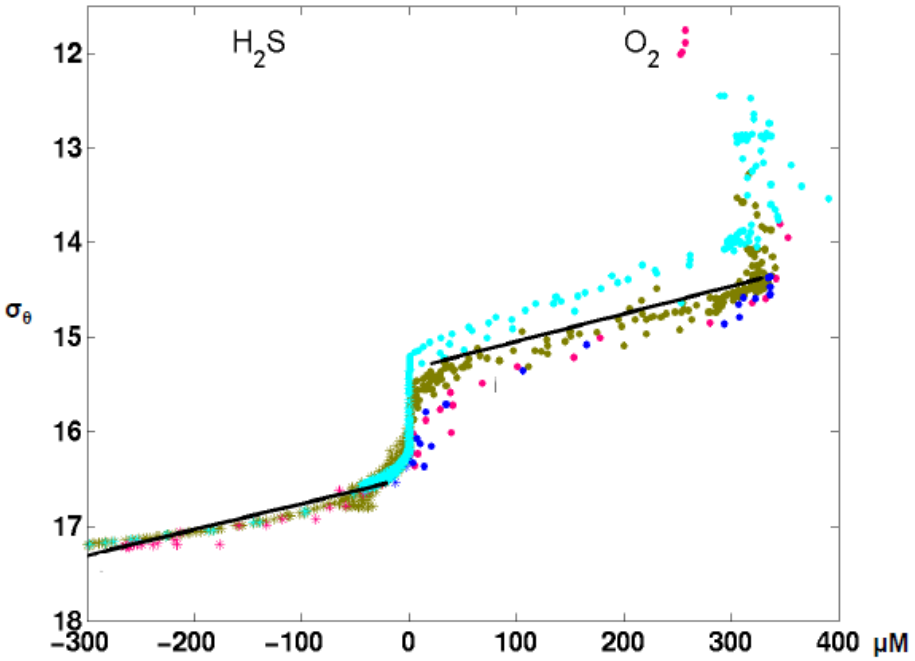

Fig. 3. Historical observations of oxygen (dots) and hydrogen sufide (stars) plotted against σ_θ. The concentrations of hydrogen sufide are multiplied by −1 in order to better illustrate how similar the gradients of oxygen and sulfide are. Regression curves are also given to illustrate the density boundaries of the suboxic layer (the *y*-intercept for zero concentrations). Data has been taken in the locations depicted in Fig. 1 by colored squares corresponding to the following surveys performed by RV *Lomonsov*, 1964.08 (red), *Atlantis*, 1969.04 (blue), *Knorr*, 2001.06 (cyan), *Knorr*, 2003.05 (brown).

BGD
11, 281–336, 2014

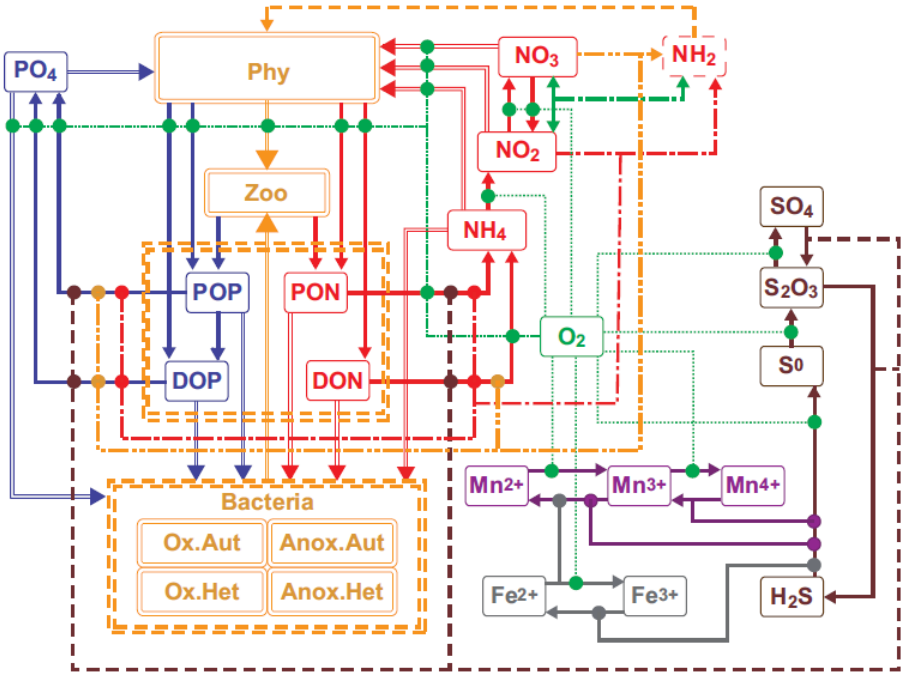

Fig. 4. Flow-chart of biogeochemical processes represented in ROLM (replotted from Yakushev et al., 2007). The names of variables and the used abbreviations are given in Table A1.

BGD
11, 281–336, 2014

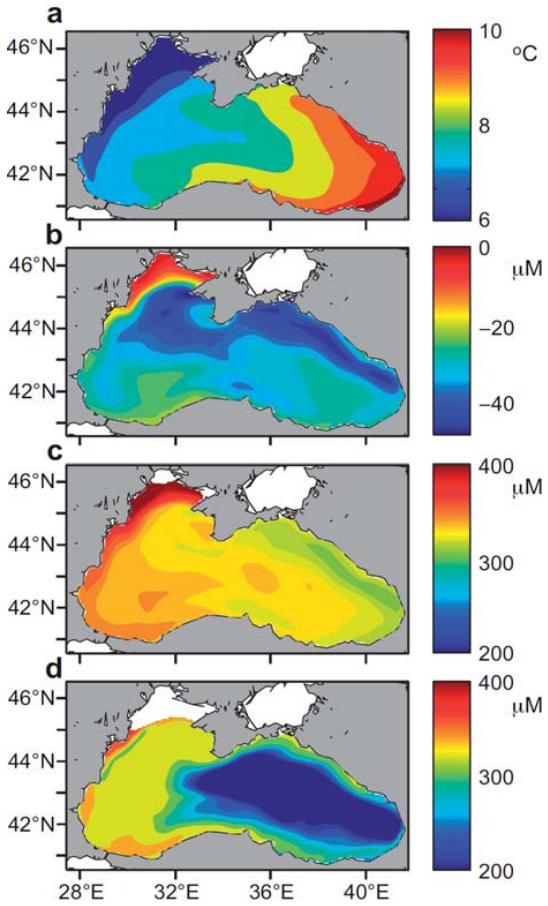

Fig. 5. Selected model results obtained for February 2010 (averaged): **(a)** SST, **(b)** difference between simulated sea surface oxygen and saturation values computed from UNESCO formula, (**c** and **d**) oxygen at 20 m, and 40 m, respectively.

BGD
11, 281–336, 2014

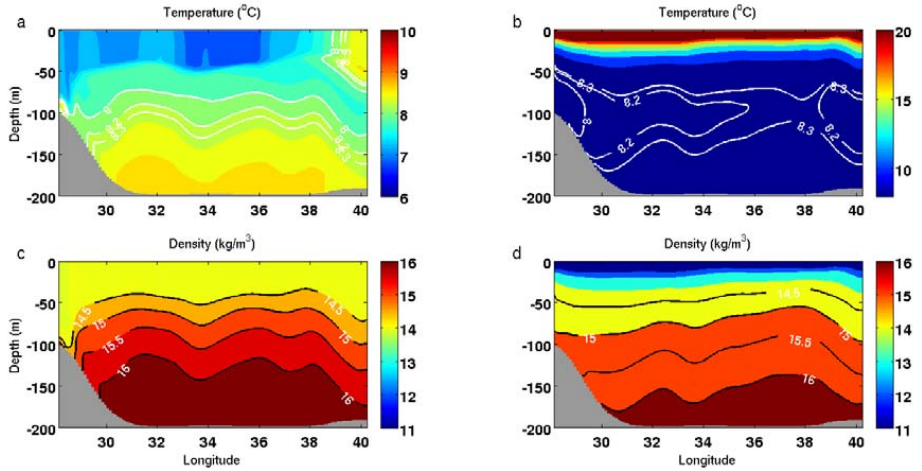

Fig. 6. Zonal cross-section at 43.3° N (see Fig. 1 for the position of the section) of temperature and density on 15 February 2010. **(a, c)** and 15 July **(b, d)** 2010. The white isolines (8, 8.1, 8.2, 8.3) depict the CIL.

BGD
11, 281–336, 2014

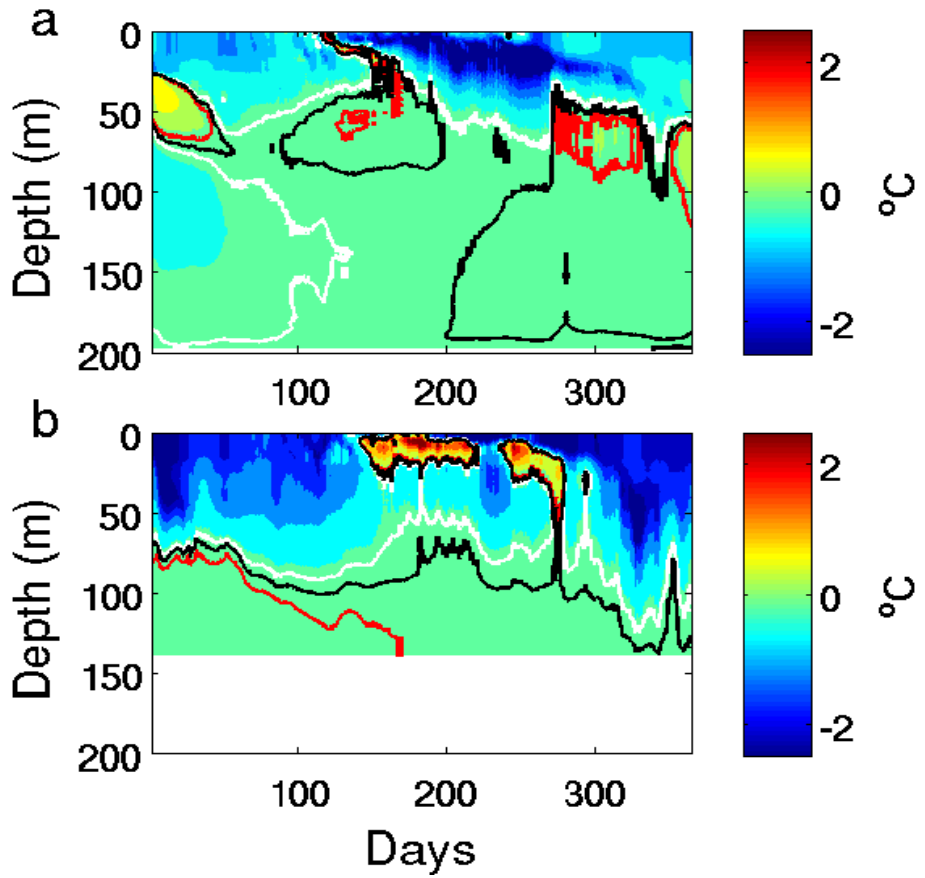

Fig. 7. Time vs. depth diagrams of the difference between current temperature profile and basin mean temperature $T(z,t)$ in 2010. **(a)** in location B, **(b)** in the coastal location A (see Fig. 1 for the positions). Isolines 0.1 °C (red), 0 °C (black) and −0.1 °C (white) were also plotted to better distinguish between positive and negative anomalies.

BGD
11, 281–336, 2014

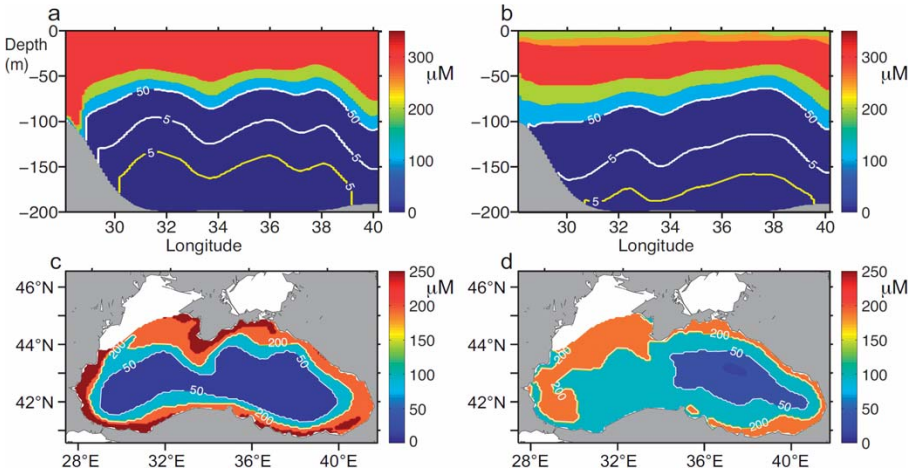

Fig. 8. Vertical cross-sections of oxygen concentrations along along 43.3° N (**a** and **b**) and horizontal distribution of oxygen at 80 m (**c** and **d**) obtained for 15 July (**a** and **c**) and 15 February (**b** and **d**) 2010. The oxygen vs. depths values have been estimated using the regression equation linking oxygen and density (derived in Fig. 3 from in-situ observations) jointly with the vertical profile of density simulated by the 3-D model in order to extrapolate the formulation throughout the basin. The white isolines of oxygen concentrations on the zonal sections are 5 and 50 μM, respectively. The yellow isolines (**a** and **b**) represent the 5 μM concentration of hydrogen sulfide..

BGD
11, 281–336, 2014

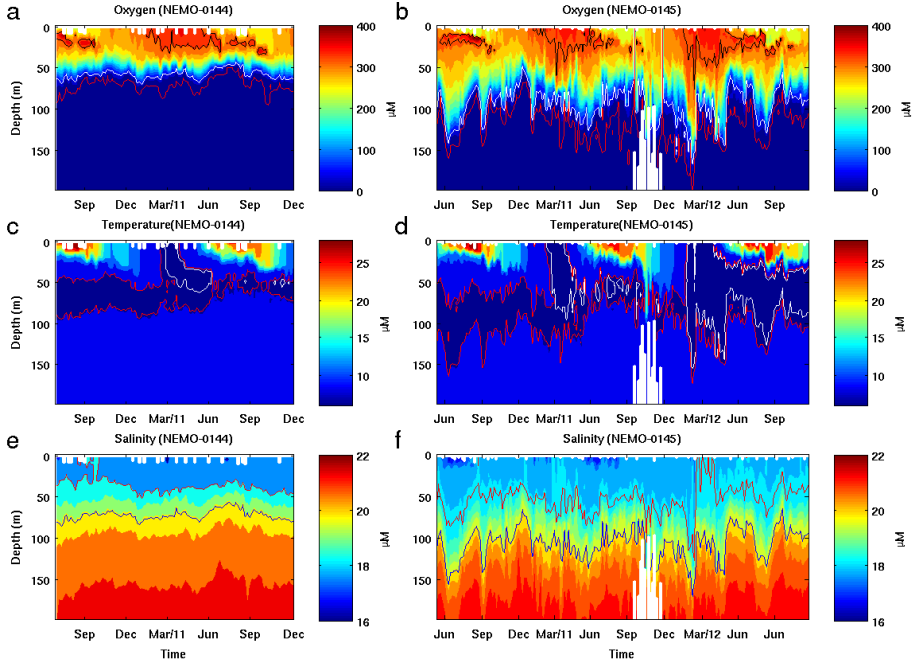

Fig. 9. Time vs. dept plots oxygen, temperature and salinity as observed by NEMO-0144 (left) and NEMO-0145 (right). (**a** and **b**) illustrate the evolution of subsurface oxygen maximum and the mesoscale variability of the suboxic layer presented by the white isolines of oxygen concentration 5 (red line) and 50 μM (white line), respectively. (**c** and **d**) in the middle illustrate the formation and evolution of the cold intermediate layer, with red and white isolines depicting temperature 8 (white line) and 8.35 °C (red line), respectively. (**e** and **f**) illustrates the temporal variability of salinity profiles, which illustrates the stability of stratification (the later tends to reduce the vertical exchange). Salinity of 18.3 and 19.9 psu are plotted with red and blue lines, respectively.

BGD
11, 281–336, 2014

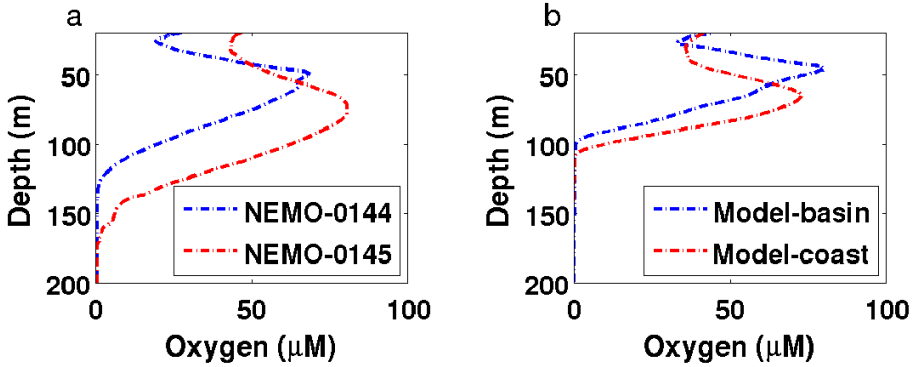

Fig. 10. (a) Standard deviation of oxygen from the mean profiles as seen in the observations of the two Argo floats (NEMO-0144 & -0145). **(b)** Standard deviation in the numerical simulations in the central basin and coastal region (positions A and B in Fig. 1). The profiles in the upper 20 m layer were not shown because of problems with the availability of the observations.

BGD
11, 281–336, 2014

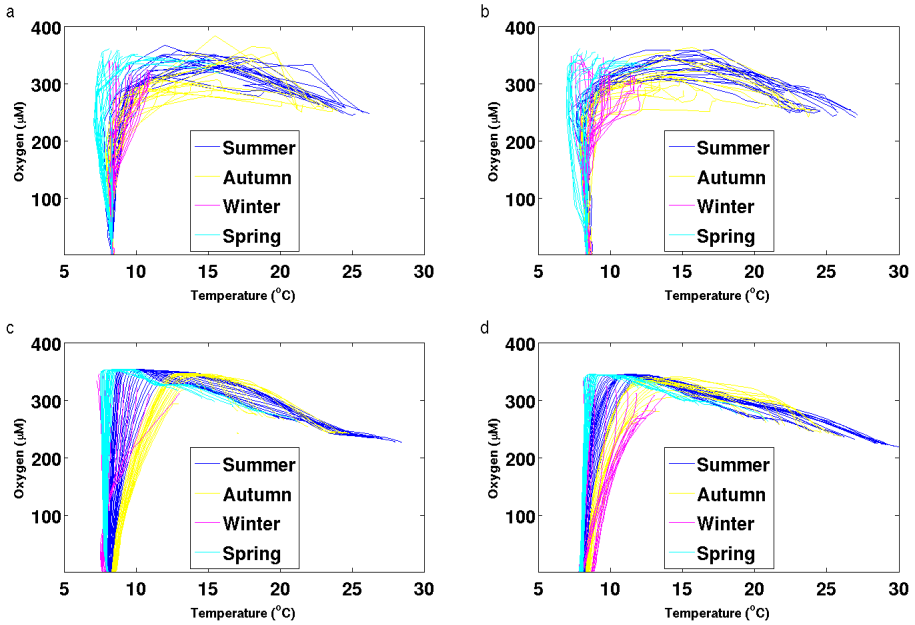

Fig. 11. Oxygen vs. temperature plots in four seasons from observations by Argo floats of NEMO-0144 **(a)** & 0145 **(b)** and from the 3-D simulations in locations B **(c)** and A **(d)**.

BGD
11, 281–336, 2014

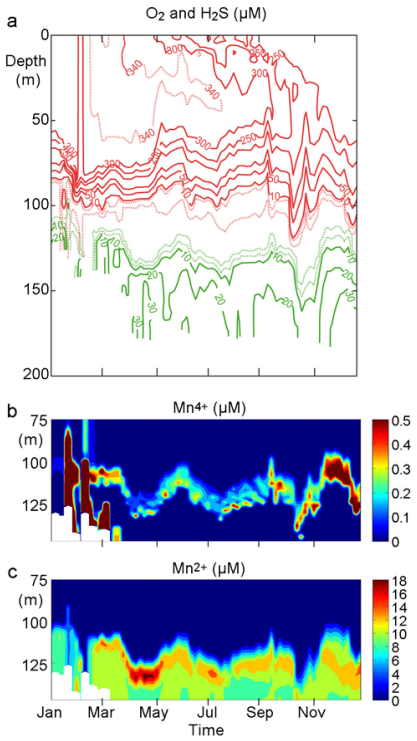

Fig. 12. Simulated seasonal variability of oxygen and hydrogen sulphide **(a)**, manganese IV **(b)** and manganese II **(c)**. The data used to plot depth vs. time diagrams were sampled from the numerical simulations for the times and positions occupied by NEMO-0145 in 2011. The first variable in **(a)**, which is the oxygen is plotted with red lines the second one (H_2S) with green lines. The dash lines are used to better trace the evolution of subsurface O_2 maximum, the dotted lines show concentrations of 5 and 1 μM O_2 and 5 and 1 μM H_2S, revealing thus the position of the suboxic zone.

BGD
11, 281–336, 2014

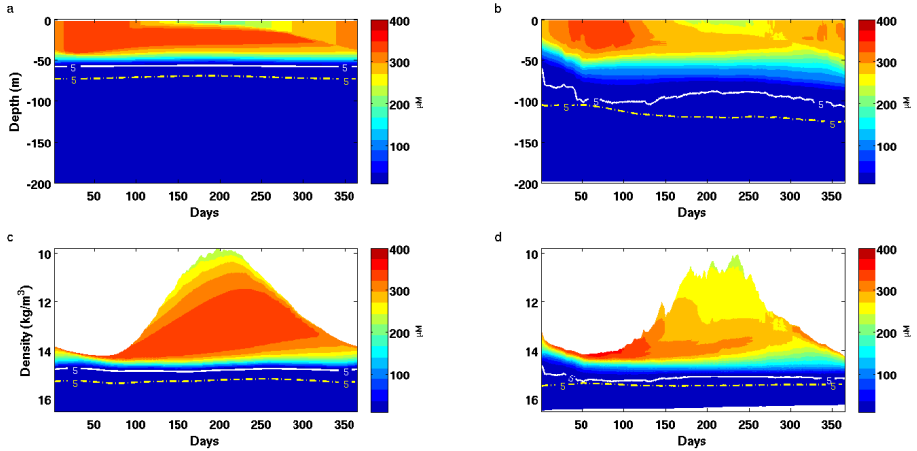

Fig. 13. Temporal evolution of the simulated in 1-D model (left) and basin mean from the 3-D model (right) oxygen concentration. **(a, b)** and **(c, d)** are representations in geopotential and density coordinates, respectively. The 5 μM H_2S isoline, which is plotted with yellow dash isolines and the 5 μM oxygen isolines (white lines) illustrate the position of the suboxic zone.

BGD
11, 281–336, 2014

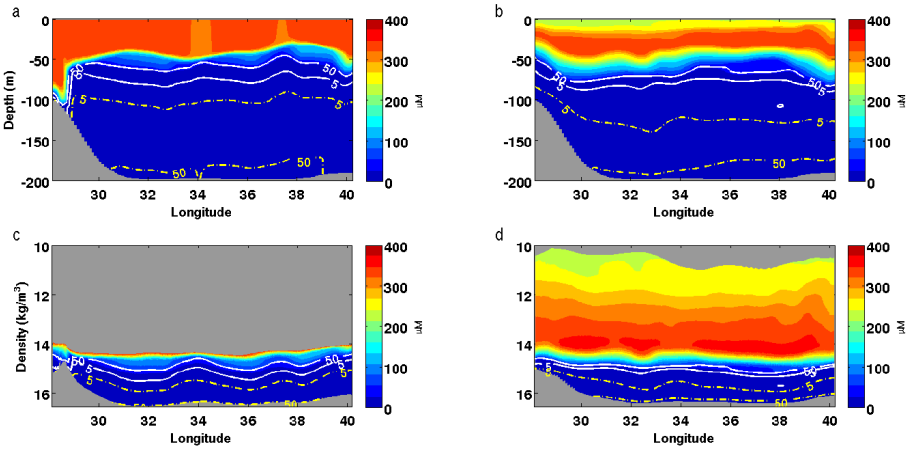

Fig. 14. Zonal cross section of oxygen simulated on 15 February **(a, c)** and 15 July **(b, d)** at 43.3° N. **(a)** and **(b)** are plotted in geopotential coordinates, **(c)** and **(d)** in isopicnic ones. The white isolines of oxygen concentrations depict 5 and 50 μM, respectively. The yellow isolines of sulfide concentrations are 5 and 50 μM, respectively.

BGD
11, 281–336, 2014

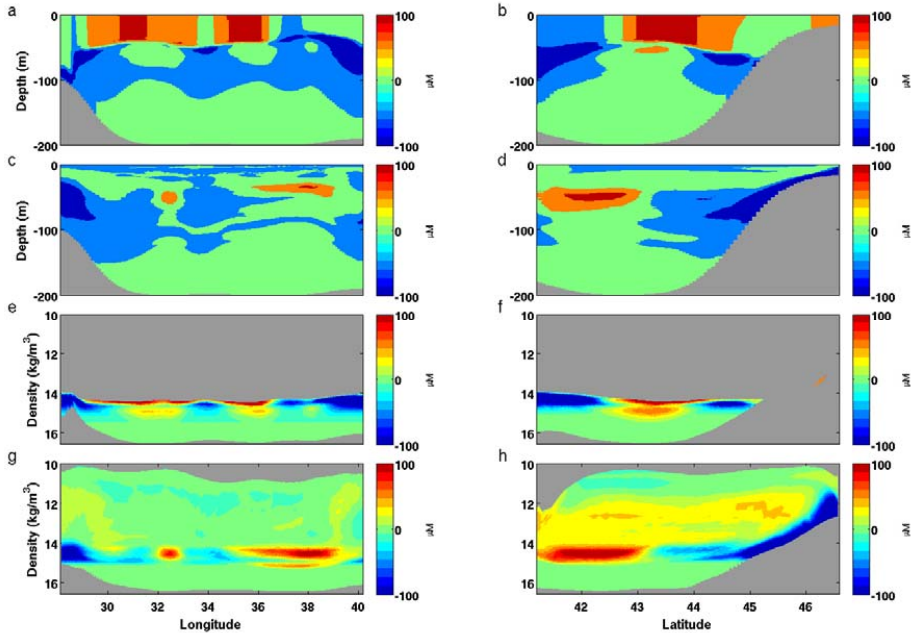

Fig. 15. Anomaly (compared to the basin wide average vertical profile) of the simulated oxygen concentrations along a zonal (at 43.3° N, **a**, **c**, **e**, **g**) and meridional (at 31.3° E, **b**, **d**, **f**, **h**) section (see Fig. 1 for the position of these sections) obtained on 15 February 2010 (**a**, **b**, **e**, **f**) and 15 July 2010 (**c**, **d**, **g**, **h**) plotted in geopotential **(a–d)** and isopycnic **(e–h)** coordinates.

BGD
11, 281–336, 2014

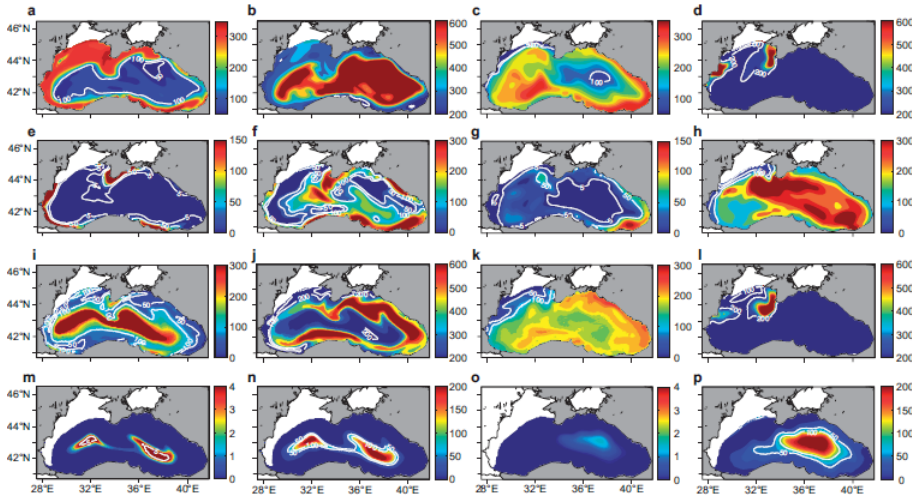

Fig. 16. Simulated concentrations of oxygen in µM and phytoplankton in mg of wet weight in cubic meter (mg WW m^{-3}) at 50 m **(a–d)** and 80 m **(e–h)**. Plots on the third and forth row show concentrations of oxygen and phytoplankton at density level 14.5 **(i–l)**, and 15.5 **(m–p)**, respectively. The first and third column show oxygen on 15 February **(a, e, i, m)**, and 15 July **(c, g, k, o)**. Similarly, the second and forth columns display phytoplankton on 15 February **(b, f, j, n)** and 15 July **(d, h, l, p)**, respectively. Oxygen isolines of 50 and 100 µM (white lines) in **(a, c, i, k)** and 5 and 50 µM (white line) in **(e, g, m, o)** are plotted to better illustrate the horizontal patterns. Phytoplankton isolines of 100 and 200 mg WW m^{-3} (white lines in **b**, **d**, **j** and **l**) and 50 and 100 mg WW m^{-3} (white line in **f**, **h**, **n** and **p**) are also plotted to better illustrate the horizontal patterns.

BGD
11, 281–336, 2014

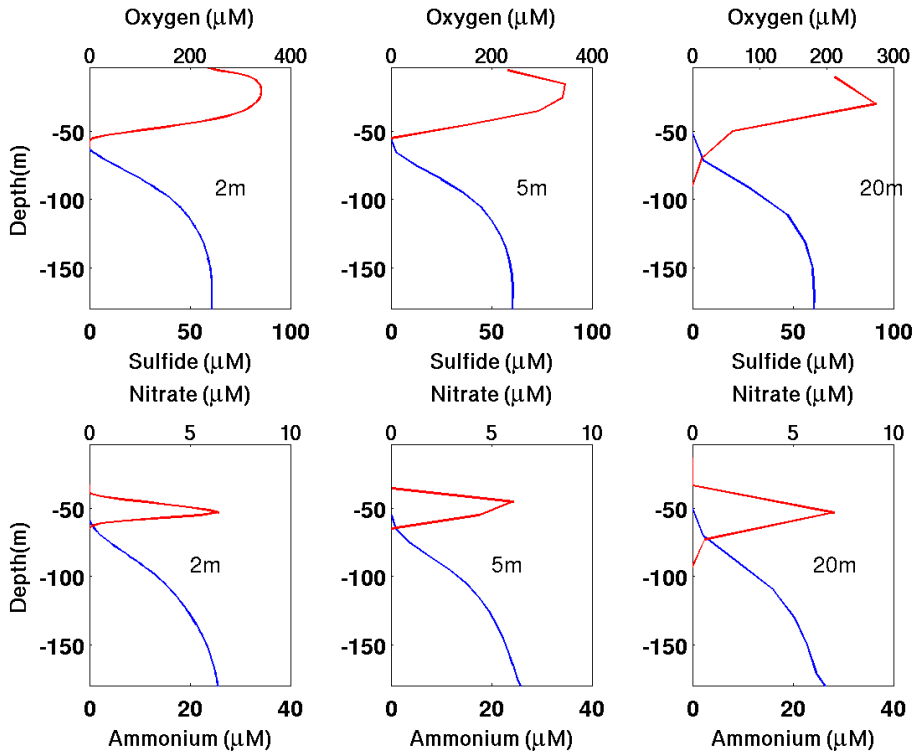

Fig. A1. Vertical profiles of oxygen (red line), sulfide (blue line), nitrate (red line) and ammonia (blue line) in 1-D simulations with different resolution of 2 m (left, experiment A), 5 m (middle, experiment B) and 20 m (right, experiment C).

BGD
11, 281–336, 2014

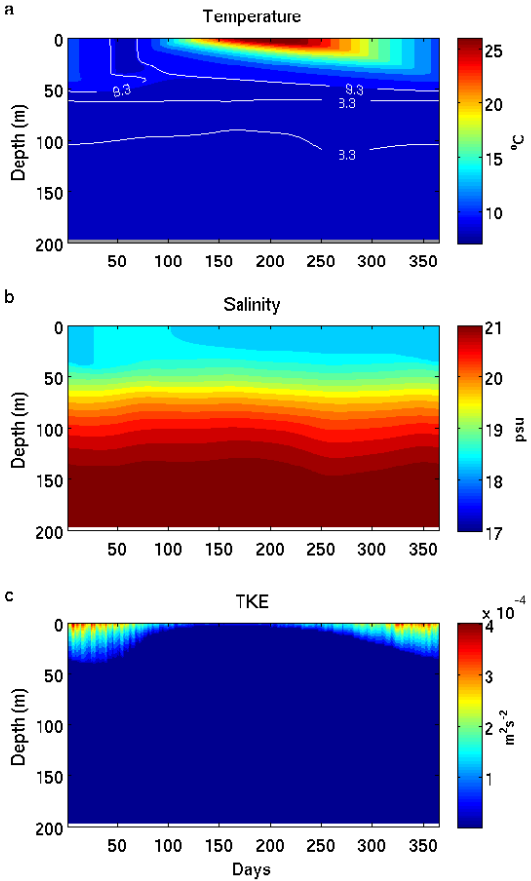

Fig. A2. Seasonal evolution of the vertical profile of **(a)** temperature (in °C), **(b)** salinity (in psu) and **(c)** turbulent kinetic energy (in $m^2 s^{-2}$) simulated in the 1-D model. The white isolines (8.3 and 9.3 °C) identify the upper and lower boundaries of the CIL.

BGD
11, 281–336, 2014